Chemical Engineering Journal Advances 17 (2024) 100579

Contents lists available at ScienceDirect

Chemical Engineering Journal Advances

journal homepage: www.sciencedirect.com/journal/chemical-engineering-journal-advances

Selective electrodeposition of Co-Ni alloys from synthetic quasi LiB NMC 532 cathode sulphate solutions using rotating plate potentiostatic electrowinning

Tendai Tawonezvi [a,b,*], Dorcas Zide [a,c], Myalelo Nomnqa [b], Leslie Petrik [a], Bernard Jan Bladergroen [a]

[a] South African Institute for Advance Materials Chemistry (SAIAMC), University of the Western Cape, Robert Sobukwe Road, Bellville, Cape Town 7535, South Africa
[b] Department of Chemical Engineering, Cape Peninsula University of Technology, Symphony Way, Bellville, Cape Town 7535, South Africa
[c] Department of Chemistry, Cape Peninsula University of Technology, Symphony Way, Bellville, Cape Town 7535, South Africa

ARTICLE INFO

Keywords:
Lithium-ion batteries
Recycling
Recovery
Valuable metals
Cobalt
Nickel, Electrowinning

ABSTRACT

The interest in recycling spent lithium-ion batteries (Li-ionB) has surged due to the rising demand for valuable metals (e.g., Co, Ni, Li and Mn) and concerns about environmental repercussions emanating from conventional battery waste disposal. This research is centered on the recovery of the valuable Ni-Co alloys from synthetic Ni, Co, Mn and Li sulphate solutions mimicking the NMC 532 ratio of elements using a hydro-electrometallurgy process route that integrates hydrometallurgy and potentiostatic electrometallurgy techniques. This quasi-model is done to elucidate the effect of multiple influencing parameters, through isolation and varying, on the selective electrodeposition of Co-Ni from multi-ion (Li, Ni, Mn and Co) complex solutions before applying it using real cathode leachates. The selective electrowinning metal recovery process route is a cost-effective alternative to the energy, cost and material-intensive hydrometallurgy intermediate purification processes such as solvent extraction, selective precipitation, and ion-exchange. The study delves into the effects of various electrowinning parameters, including applied potential, temperature, pH, Co, Ni, Na_2SO_4, NaH_2PO_4 buffer concentration, and cathode rotational speed. These parameters were thoroughly investigated and effectively optimised to achieve the recovery of 98.2% pure $Ni_{0.65}Co_{0.35}$ at a rate of 0.060 g/cm^2.h with an impressive 89.25 % current efficiency. The composition of the electrowon deposit was meticulously quantified using Inductively Coupled Plasma Optical Emission Spectroscopy (ICP-OES) and subjected to analysis through a Scanning Electron Microscope (SEM-EDS). Additionally, the phase composition was evaluated using X-Ray Diffraction analysis (XRD). The results successfully demonstrate the technical feasibility of recovering Ni-Co alloys, yielding high quantities of industrial-grade pure Ni-Co alloys. This comprehensive electro-hydrometallurgical process, designed for both closed and loop recycling purposes, promotes a more environmentally preservative approach to recycling spent lithium-ion battery cathode material. The approach contributes significantly to the development of sustainable resource management infrastructure.

Introduction

Lithium-ion batteries (Li-ionBs) have gained significant popularity as a multipurpose commercial rechargeable battery option primarily due to their exceptional electrochemical properties, including but not limited to high energy density, high operating voltage, zero memory effect, compact unit size, low self-discharge rate, and a wide range of operating temperatures [1]. The extensive production and application of Li-ionBs have led to an enormous amount of spent Li-ionBs due to their relatively limited life spans and the periodic upgrades of electronic technology products. These spent Li-ionBs constitute large amounts of valuable metals ranging from Ni, Co, Ni, Mn, Cu, Al, and Fe [2,3]. Typically, they consist of Co in the 5–20 wt% range, Li in the range of 5–8 wt.%, Ni in the range of 5–20 wt.%, organics in the range of 5–15 wt.%, and plastics in the range of 3–7 wt.% [3–8]. Moreover, the organic electrolytes and heavy metals used in the spent Li-ionBs comprise toxic components that

* Corresponding author at: South African Institute for Advance Materials Chemistry (SAIAMC), University of the Western Cape, Robert Sobukwe Road, Bellville, Cape Town 7535, South Africa.
E-mail address: tendaitawonezvi@yahoo.com (T. Tawonezvi).

https://doi.org/10.1016/j.ceja.2023.100579

Available online 1 December 2023

could harm human and environmental health if disposed of improperly. That is, if Li-ionBs are disposed of using the simple yet inapt conventional treatment methods (e.g., landfill), detrimental environmental pollution such as groundwater and soil contamination caused by the leakage of hazardous materials will unravel [4,6,9–11].

Up to date, numerous process routes have been developed for the recovery and recycling of valuable metals and materials from spent Li-ionBs. These process routes include pyrometallurgical, hydrometallurgical, and electrometallurgical processes. The pyrometallurgical processes are often integrated with hydrometallurgical processes to recycle valuable components, materials and metals. Electrometallurgy utilizes electrical current and voltage to extract metals from their ore solutions [2,12]. It is conventionally the last stage in valuable metal extraction and is therefore preceded by pyrometallurgical and/or hydrometallurgical process stages [1]. Closed-loop recycling has been demonstrated to be efficient and cost-effective within specific industries but has limited versatility in terms of repurposing materials whilst open-loop recycling, which offers greater material versatility and potentially reduces waste in the long term, tends to be more expensive and energy-intensive due to the need for extensive processing and transportation [13,14]. In addition to the above, it is worth noting that most recycling work up to date is open-loop recycling since most of the valuable metals will be repurposed for multiple and broad applications.

In this work, Ni-Co alloys from synthetic spent Li-ionBs NMC 532 sulphate solutions were recovered through an integrated hydrometallurgy and electrometallurgy process for closed and open loop recycling since besides Li-ioB cathode production, which is the main target use for the Ni-Co, Ni-Co alloys and alloys can be used in magnetic films, electrocatalysis, electronic chips, anti-corrosion systems, micro and nano-gears among other various technological applications [15,16]. This quasi-model is done to elucidate the effect of multiple influencing parameters, through isolation and varying, on the selective electrodeposition of Co-Ni from multi-ion (Li, Ni, Mn and Co) complex solutions before applying the developed model using real Li-IonB cathode leachates. Conventionally, galvanostatic electrowinning is utilized to reduce metallic ion solutions, pure metal solutions that are produced by hydrometallurgy intermediate separation processes like solvent extraction, ion exchange and selective precipitation. The rationale of this research is hinged on fostering direct potentiostatic electrowinning as a cost-effective selective metal recovery alternative, not as part of the multistage conventional metal processes, for hydrometallurgy intermediate separation processes like solvent extraction, ion exchange and selective precipitation (to produce pure metal io solutions) to reduce cost, utilization of potentiostatic techniques (instead of galvanostatic) to selectively extract specific metals and enhance the purity and lastly, utilization of platinum coated titanium dimensionally stable anodes (DSA) to reduce contamination and levelized cost of operation, utilising optimised operational parameters to reduce energy consumption and operational cost and utilization of rotating cathode to increase cathode density and ultimately recovery yield. The reduction potentials of the metals found in the cathode are listed as follows:

$$Co^{2+} + 2e^{-} \rightarrow Co \; E = -0.28 \; (V \; vs \; SHE) \quad (1)$$

$$Ni^{2+} + 2e^{-} \rightarrow Ni \; E = -0.25 \; V \; (V \; vs \; SHE) \quad (2)$$

$$Li^{3+} + 2e^{-} \rightarrow Li \; E = -3.04 \; (V \; vs \; SHE \quad (3)$$

$$Mn^{2+} + 2e^{-} \rightarrow Mn \; E = -1.2 \; (V \; vs \; SHE) \quad (4)$$

It is believed that through applying specific constant potential for Co and Ni (potentiostatic electrowinning), Ni and Co can be selectively separated from Li and Mn. It is believed that through applying specific constant potential applicable selectively for Co and Ni reduction (potentiostatic electrowinning), Ni and Co can be selectively separated from Li and Mn. The integrated hydro-electrometallurgy process route of extracting Ni-Co alloys was explored and thoroughly assessed. The results demonstrate the technical viability of recovering Ni and Co through the optimised hydro-electrometallurgy process.

Experimental

Materials

In our set of experiments, the source of materials was the Li-ionBs (NMC 532) cathode material sourced from our in-house lab (ESIL, South Africa). The reagents cobalt sulphate (98%, Kimix, South Africa), nickel sulphate (99%, Sigma Aldrich, South Africa), sulphuric acid (98%, Alfa Aesar, USA), titanium plate (99%, Sigma Aldrich, USA), manganese sulphate (98%, Sigma Aldrich, USA), sodium sulphate (98%, Kimix, South Africa), hydrazine nonohydrochloride (97%, Sigma Aldrich, USA), hydrogen peroxide (50% Kimix, South Africa), hydrochloric acid (37 %, Alfa Aesar, USA), chloroplatinic acid (Sigma Aldrich, USA) and monosodium phosphate (98%, Sigma Aldrich, USA) were purchased and used without further purification.

Material characterisation

The diffraction patterns of the cathode material (88.5 % active material + 11.5% (binder + Al-foil + carbon powder) were recorded using a multipurpose X-ray Diffractometer D8-Advance from BRUKER AXS (Germany). Measurements were operated in a continuous θ - θ scan in locked coupled mode with Cu-Kα radiation (λKα1=1.5406 Å) in the 2-theta ranged from 5° to 90°, in steps of 0.034° per second. The morphology and elemental composition of the cathode material were further confirmed using scanning electron microscopy (SEM) coupled with energy-dispersive X-ray spectroscopy (EDS). The elemental analysis was determined using inductively coupled plasma optical emission spectroscopy (ICP-OES).

Leaching and elemental analysis

The leaching of NMC 532 was optimised in-house but not reported in detail in this work. The leaching optimisation experimental work determined the optimal conditions for leaching Co, Ni, Mn, and Li from spent Li-ionB cathodes ($LiNi_{0.5}Mn_{0.3}Co_{0.2}O_2$). Through the utilization of leachate solutions comprising 2 M H_2SO_4 + 6 vol.% H_2O_2, and a 75 g/L S/L ratio, and conducting leaching for 120 min at a temperature of 60 °C, the recovery efficiency of 98.1 % for Li, 97.1 % for Co, 96.1 % for Ni, and 95.7 % for Mn were achieved as shown in Table 1. The maximum metal recovery that was attained is 0.595 $g_{total\ metal}/g_{cathode}$. Table 2 tabulates the composition of a leached Li-ionB ($LiNi_{0.5}Mn_{0.3}Co_{0.2}O_2$) using a 75 g/L S/L ratio, 2 M H_2SO_4 + 6 H_2O_2 v/v% solution at 60 °C for 2 h and an identical synthetic Ni, Mn, Co and Li sulphate solution.

Electrowinning recovery of Ni-Co composite

The single-compartment electrowinning cell consisted of a Pyrex 360 ml jacketed cylinder with a Perspex cover holding the 3 electrodes. The cathode slot was fitted with a Metrohm rotating motor. Initial electrowinning optimisation tests were conducted in a jacketed reactor vessel using a synthetic $Co^{2+}_{0.3}Ni^{2+}_{0.7}$ solution (made from mixing 5.25 g

Table 1
Composition of a leached Li-ionB ($LiNi_{0.5}Mn_{0.3}Co_{0.2}O_2$) using a 75 g/L S/L ratio, 2 M H_2SO_4 + 6 H_2O_2 v/v% solution at 60 °C for 2 h and synthetic Ni, Mn, Co and Li sulfate solution.

Element	[g/L] (NMC 532)	g/L (Synthetic)
Li	4.98	5.5
Ni	19.94	21.0
Co	8.214	9.0
Mn	11.59	12.0

Table 2
Chemical composition, determined by ICP-OES and EDS, of the deposit obtained in the electrowinning (30 g/L $Co^{2+}_{0.3}Ni^{2+}_{0.7}$, −1.15 V vs Ag/AgCl, 50 °C, 40 rpm, 15 g/L of buffer, 15 g/L Na_2SO_4, pH 4.5).

	Weight % (Before EW)	Weight % (After EW) [AA/EV of 2 m^2/250 cm^3]		Weigh % (After EW) [AA/EV of 30cm^2/ 250 cm^3]		Recovered [%]
		EDS	ICP	EDS	ICP	
Co	18.5	59.82	69.09	27.16	34.97	90
Ni	44.6	27.51	32.63	62.67	66.45	75
O	-	13.46	-	10.21	-	
Mn	25.9	1.51	1.78	1.58	1.86	4.1
S	-	0.46	-	0.51	-	-
Na	-	0.29	0.35	0.31	0.39	-
Li	11.1	0.03	0.05	0.03	0.06	0.8

$NiSO_4{\cdot}7H_2O$ and 2.25 g $CoSO_4{\cdot}7H_2O$ in 250 ml) to determine the optimal conditions for Co^{2+} and Ni^{2+} deposition. All synthetic solutions contained an unvaried 5 g/L of Li^+ and 12.5 g/L of Mn^{2+}. An Aluminium plate (5052 aluminium alloy) with 2 cm^2 active surface area was used as a cathode. A single platinum-coated titanium plate, made by the electroless Pt coating method reported by Rao and Pushpavanam [17], with a 4 cm^2 exposed surface area was used as the anode. The distance between the electrode planes is 1 cm and the tip of the reference electrode is positioned 0.75 cm from the anode and 0.75 cm from the cathode in a triangular set up, providing sufficient space for the electrode to rotate. The Ag/AgCl in saturated KCl reference electrode was utilized throughout all electrowinning experiments. The effect of different electrowinning parameters (pH, temperature, potential, concentration, buffer dosage, cathode rotating speed and Co/Ni ratio) on current efficiency and deposit composition and quality was studied to establish optimal levels. The electrowinning parameters were optimised using a combination of factorial design and sequential experimental design. Cyclic voltammetry studies were conducted at a scan rate of 2.5 mV/s from -1.2 to -0.2 V (vs Ag/AgCl), a temperature of 55 °C and a pH of 4. An aluminium plate with 2 cm^2 active surface area was used as the working electrode. A single platinum plate with a 2 cm^2 exposed surface area was used as the anode. The anode was positioned on the opposite facial side of the cathode with the reference electrode Ag/AgCl reference electrode) in the middle.

The optimized parameters conditions (-1.15 V vs Ag/AgCl, 30 g/L $Co^{2+}_{0.3}Ni^{2+}_{0.7}$, 50 °C, 15 g/L of monosodium phosphate, 15 g/L Na_2SO_4, pH 4.5 and Cathode Rotating Speed (CRS) of 40 rpm) determined using synthetic solutions were to be utilized in the Co-Ni composite electrowinning studies of the leachate solution obtained using an actual Li-ionB NMC 532 cathode.

Titanium was coated by platinum using the electroless deposition method by Rao and Pushpavanam [17]. An aluminium plate with a 2 cm^2 active surface area was used as a cathode coupled with a single platinum-coated titanium plate with a 4 cm^2 exposed surface area was used as anode for the 2 cm^2/250 cm^3 cathodic surface area to electrolyte volume ratio (AA/EV) set-up. An aluminium plate of (10 × 3) 30 cm^2 surface area was used as cathodes coupled with two layered platinum-coated titanium sheets measuring 10 × 3 cm which were used as anodes placed on opposite facial sides of the cathode for the 30 cm^2/ 250 cm^3 AA/EV set-up. The Ag/AgCl reference electrode, coupled with anode and cathode, was utilized in a 3-electrode sytstem throughout all the labscale batch electrowinning experiments (Fig. 1).

To determine the current efficiency, the weight of the Al-cathode was measured before and after each experiment, and the difference in mass represented the mass of the deposited Co-Ni material. However, to ensure that this mass difference accurately reflected the deposit's mass only, the cathode and the deposit were thoroughly rinsed with acetone. Then air dried using pressurized air to eliminate any traces of residual electrolyte solution adhering to the electrode-deposit matrix. The current efficiency was calculated according to the equations below:

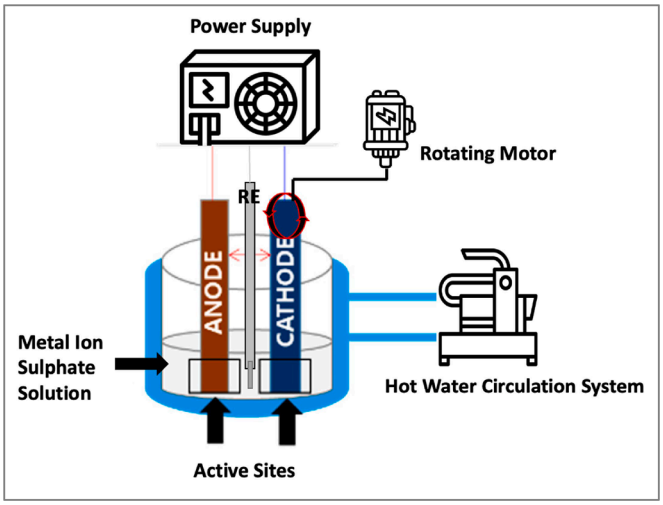

Fig. 1. Single-compartment cell used in the different electrowinning tests.

$$\eta = \frac{m_o}{m_e} \times 100 \tag{5}$$

and:

$$m_e = \frac{MIt}{nF} \tag{6}$$

Where m_o is mass obtained from electrowinning, m_e is the calculated theoretical mass at 100 % faradaic efficiency, M is molar mass, I is the current in amperes, t is the time in seconds, n is the oxidation state, and F is the faradays constant.

Results and discussion

Electrowinning optimization studies

Cyclic voltammetry for Co and Ni deposition

The potentiostatic electrowinning process is operated at a constant potential synonymous with the desired reaction. It is, therefore, imperative to determine the appropriate potential for the Ni-Co composite deposition reaction before the actual operation of the electrowinning reactors using real Li-ionB cathode leachates. The practice is to quickly assess the current vs voltage using a voltammogram for a particular electrochemical system determined at a specific concentration of electrolyte, pH and temperature. The voltammetry analysis was done at pH= 4, 50 °C and cathodic surface area to electrolyte volume ratio (AA/EV) of 2 cm^2/250 cm^3. For the Al alloy anode, voltammograms were created for the reactions of Co to Co^{2+}, Ni to Ni^{2+}, and oxygen evolution in their respective 15 g/L metal sulphate solutions spanning potential ranges of -1.2 to -0.2 and -0.2 to -1.2 V (vs Ag/AgCl).

Fig. 2(a) shows the characterization of the electrochemical of Co and Ni in their respective synthetic Co and Ni sulphate electrolyte solutions using Al cathodes at a scan rate of 2 mV/s. Fig. 2(b) depicts the analyzes of the electrochemical behavior of Al cathodes in a 30 g/L $Ni^{2+}_{0.7}Co^{2+}_{0.3}$ solution.

Fig. 2(a) shows two anodic peaks when scanned in the positive direction for both the Co and the Ni voltammograms. In addition, Co exhibited one defined cathodic peak when scanning in a negative direction similar to the Ni voltammogram that shows one defined cathodic peak in the same potential window while demonstrating slightly higher current intensity. The trend is similar to what is reported in the literature [18–21]. The anodic peaks on the Ni and Co voltammogram, when scanning in the positive direction, also occur in the same potential window [19–21].

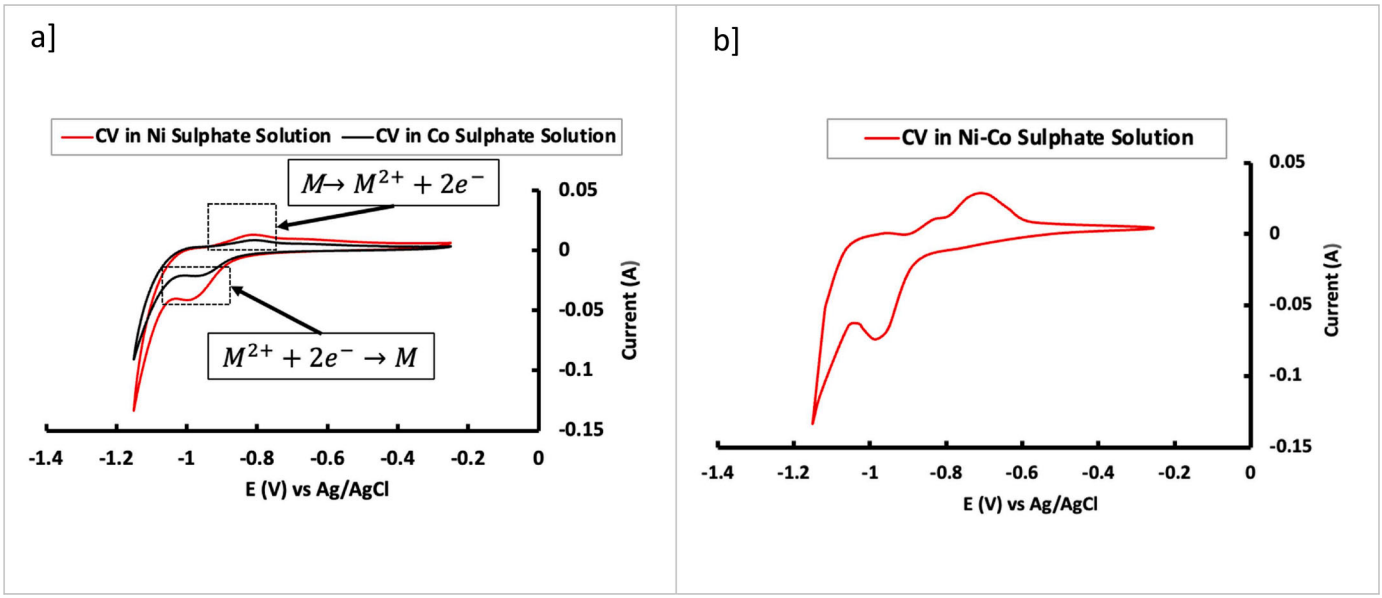

Fig. 2. Voltammograms of (a) Co and Ni deposition on Al cathode in 15 g/L metal ion solution at pH= 4 and 50 °C and (b) Co-Ni deposition on Al cathode in 30 g/L $Ni^{2+}_{0.7}Co^{2+}_{0.3}$ solution at pH= 4.

On the Co voltammogram, the first anodic peak (at -0.8), which occurs when scanning in the positive direction, is the anodic dissolution of Co (0) to Co (II), and the broad peak (at -0.6) is the further oxidation of Co (II) to Co (III) (leading to the formation of Co_2O_3 layer), which has passivating properties, followed by a broad passive region [18–21]. As the anodic potential increases to more positive values (over −0.4), Co dissolution continues, and with a further increase in the potential, O_2 evolution commences from around -0.2 V [19–21]. Oxygen evolution intensifies with the increase in cycle number [19–21]. The cathodic peak, which appeared at -0.95 V in the reverse scan (negative scan), could be attributed to the reduction of Co (II) to Co (0) formed on the Al surface interface [18,19,21].

On the Ni voltammogram, the first anodic peak (at -0.75), which occurs when scanning in the positive direction, is the anodic dissolution of Ni to Ni(II), and the broad peak (at -0.55) is the further oxidation of Ni (II) to Ni(III) (leading to the formation of Ni_2O_3 layer), which has passivating As the anodic potential increases to more positive values (over -0.4 V), Co dissolution continues, and with a further increase in the potential, O_2 evolution commences in the region of over -0.2 V [22]. Oxygen evolution intensifies as the cycle number increases [22,23]. The cathodic peak, which appeared at -0.95 V in the reverse scan (negative scan), could be attributed to the reduction of Ni (II) to Ni (0) formed on the Al surface interface [22]. Based on the above information, it is evident that Ni and Co exhibit similar electrochemical behavior, as can be seen in Fig. 2(b), which indicates only one defined cathodic peak and only one anodic peak, attributable to similar reduction and oxidation potentials for both metals which overlap therefore forming one defined and yet broad cathodic and anodic peaks. This phenomenon indicates that Co and Ni can Co deposit from a Co^{2+}/Ni^{2+} sulphate electrolyte.

Effect of Co/Ni ratio on current efficiency and deposit composition

Following the composition analysis of the deposit from the cyclic voltammetry of 30 g/L $Ni^{2+}_{0.7}Co^{2+}_{0.3}$ solution, the deposit constituted a Co/Ni ratio of 2.45, whilst the electrolyte constituted a Co/Ni ratio of 0.4. The anomalous behavior of iron-triad metals was examined by studying the effect Co/Ni ratio in the electrolyte on Co/Ni co-deposition.

Fig. 3 illustrates the effect of the Co/Ni ratio on current efficiency and deposit composition. As depicted in Fig. 13, the cobalt content in the deposit is always higher than that of the cobalt concentration in the electrolyte bath. The slight increase in the Co/Ni ratio in the electrolyte

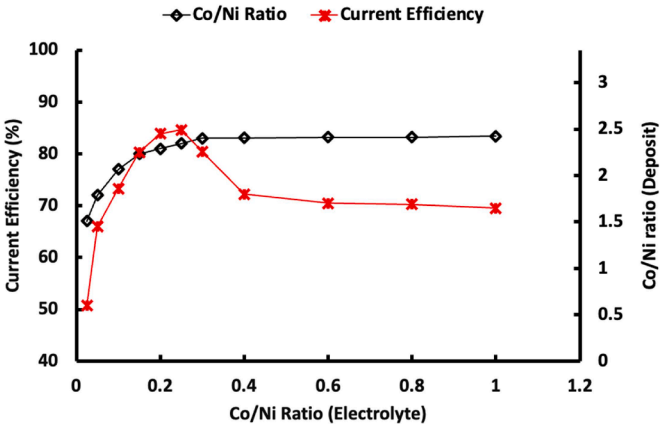

Fig. 3. The effect of Co/Ni ratio on current efficiency and deposit composition (-0.95 V, pH =5, 70 °C, 30 g/L $Co^{2+}_{0.3}Ni^{2+}_{0.7}$ and AA/EV of 2 $cm^2/250\ cm^3$).

results in an exponential rise of cobalt content in the deposit. For example, at a Co/Ni ratio of 0.1, the deposit constituted a Co/Ni ratio of 0.92, while at a Co/Ni ratio of 0.5, the cobalt content was 73 % at pH of 4, -0.95 V vs Ag/AgCl and AA/EV of 2 $cm^2/250\ cm^3$. Thus, for the Ni-Co composite, we have an unambiguous indication of inhibiting the electrodeposition of the more noble metal (Ni) and promoting the electrodeposition of the less noble metal (Co). A similar trend was observed by Golodnitsky et al. [24]. Aside from the evident effect of the Co/Ni ratio on the anomalous co-deposition of Ni and Co, it was found that the electrowon Ni/Co deposit composition of the Ni-Co electrowinning systems was also sensitive to the applied potential (Discussed in the next section).

The extent to which the current efficiency and cobalt content is affected by applied potential depends strongly on the Co/Ni ratio in the electrolyte. This intricate nature of the dependence is presumably related to diffusion limitations and changes in the composition of metal complexes, which are formed in the bulk of the electrolyte and electrical double layer at the electrode-electrolyte interface [24]. Golodnitsky et al. [24] added that the inhibiting effect on the code position of the more noble metal is generally strongest when the reaction rate of the less noble metal is kinetically controlled and diminishes as the limiting

current is reached.

The Co-Ni composite current efficiency reaches a maximum at a Co-Ni ratio in the electrolyte equal to 0.25 ± 0.03, corresponding to approximately 22–28 % of cobalt content in the Co-Ni composite (Fig. 3). The maximum of the current efficiency coincides with the formation of the more sophisticated structure of the Ni-Co composite. The further decrease of current efficiency as a function of Co^{2+} concentration in sulphate electrolyte may be attributed to the decline in hydrogen evolution overpotential on the cobalt-rich alloys resulting in hydrogen evolution side reaction.

Partial polarization curves of Ni^{2+} and Co^{2+} co-deposition presented by Golodnitsky et al. [24] indicated that after an increase of cobalt (II) concentration in the electrolyte by a factor of 16, the peak curve is accompanied by the positive (0.2 V) shift of the cobalt reduction potential whilst the opposite effect (-0.5 V) was found for Ni (II) co-deposition. This shift indicates that Co deposition is more favored as the concentration of Co^{2+} in the electrolyte increases. Changes in temperature, pH and bath composition do not influence the Tafel slope of Co and Ni deposition reactions [24,25]. The cathode reactions were found to be first order with respect to Ni^{2+} and Co^{2+} concentrations, which entails a two-stage process, where the rate-determining step is the acquisition of the first electron [24]. Additional support for this assumption is Ni-Co alloy deposition's large apparent activation energy15.5 kcal/mol) [24,25].

To elucidate the anomalous co-deposition of N^{i2+} and Co^{2+}, it is worth considering the formation of the individual complexes from the standpoint of crystal-field theory [26]. In light of this theory, Ni^{2+} and Co^{2+} complexes can be related to coordinative substances whose structures show slight sublevel splitting, which are high-spin complexes. This possible deduction points to the fact that inhibiting the discharge rate of the nobler component is likely to depend on the internal structural features of $Ni^{2+}$and Co^{2+} species involved in the reduction process.

To further explain the anomalous co-deposition of $Ni^{2+}$and Co^{2+}, it is pre-eminent to consider the individual metallic ion complexes from the standpoint of the crystal-field theory. Cobalt has the electronic structure $3d^74s^2$, while nickel has the electronic structure $3d^84s^2$. In the light of this theory, aquo- and protonated sulpha-mated Ni^{2+} and Co^{2+} complexes can be related to coordinative substances, whose structures show slight sublevel splitting, namely, high spin complexes [24,25,15]. The calculated crystal field stabilization energy for Ni^{2+} in octahedral complexes is 29.3 and 17.1 kcal for Co^{2+}.

High-spin octahedral Co^{2+} complexes with three unpaired electrons are more labile than Ni^{2+} [27–29]. Therefore, the formation of high-spin Co^{2+} complexes is more feasible (than high-spin Ni^{2+} complexes) and is expected to react rapidly. The appearance of labile high-spin cobalt complexes is believed to explain the preferential reduction of Co^{2+} compared to Ni^{2+}. Moreover, high-spin complexes involved in the reaction would permit a two-step reduction mechanism, which is in complete agreement with the experimentally modelled Tafel slopes by Golodnitsky et al. (1998). Even though the actual electrode reactions of electrochemical alloying of the iron-group metals may include additional intermediate steps, we believe that in the first approach, the crystal-field theory permits generalization for anomalous co-deposition of $Co^{2+}$and $Ni^{2+}$from different electrolytes. Along with competitive adsorption and underpotential deposition, the crystal-field theory can be considered one possible explanation for the unsuspected behavior of electrochemical alloying of iron-triad metals.

Effect of applied potential on current efficiency and rate of deposition

The investigation of the effect of potential on the mean current as a

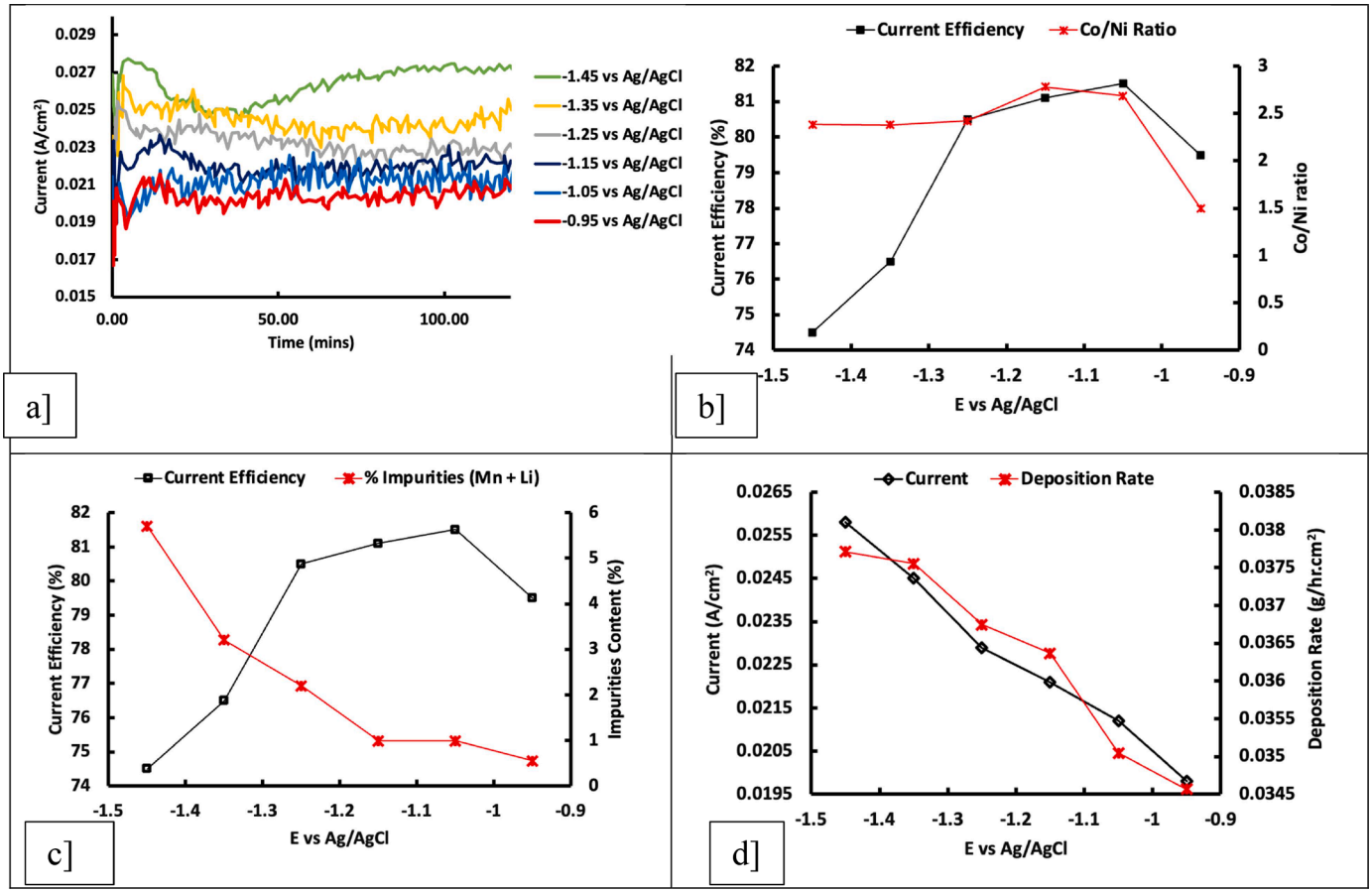

Fig. 4. Effect of applied potential on (a) on the mean current as a function of time, (b) current efficiency and rate of deposition, (c) current efficiency and% impurity and (d) the mean current (tests done at pH=5, 60 °C and 2 cm^2/250 cm^3 AA/EV in 30 g/L of 47.5 g/L $Co^{2+}_{0.25}Ni^{2+}_{0.1}Mn^{2+}_{0.15}Li^{+}_{0.5}$.

function of time is depicted in Fig. 4(a). Evidently, the mean current increases with an increase in applied potential. The investigation of potential against the rate of deposition demonstrated a positive correlation, indicating that higher applied potentials resulted in increased rates of deposition (Fig. 4(d)). The highest deposition rate was found to be 0.0385 g/hr.cm^2 at current 0.255 A/cm^2, potential of -1.45 V (vs Ag/AgCl) and 1 cm cathode-anode distance. As the potential increases, more electrons are availed for the deposition reaction (metal ion reduction reaction), leading to increased deposit formation. Since the surface of the cathode became irregular at high deposition rates, and the supplementary deposited mass could not stick to the cathode, the impurities could easily be deposited along with Co and Ni; therefore, it is not advisable to operate at high potentials (as shown in Fig. 5(c)).

The deposition rate-potential curves exhibit similar trends to current-potential curves, as seen in Fig. 4(d), since more active electrons are availed for the Co^{2+} reduction at higher applied potentials and currents. In the region where the curves are steep, after the limiting overvoltage, the system becomes unstable, and the liberation of hydrogen produces a spongy-cobalt deposit onto the cathode as depicted by Fig. 5(c) indicates that the impurity composition increases with applied potential due to the non-selective reduction of impurity species on the cathode at higher applied potentials.

Fig. 4(b) shows that the Co/Ni ratio increases from 1.5 to 2.5 when the potential increases from -0.95 to -1.05; thereafter the Co/Ni ratio stabilizes with negligible deterioration. The Co-Ni composite current efficiency reaches a maximum (81%) at -1.05 V vs Ag/AgCl. The maximum of the current efficiency coincides with the formation of the more sophisticated structure of Ni-Co composite at higher potentials. Further decrease of current efficiency as a function of Co^{2+} concentration in sulphate electrolyte may be attributed to the reduction of hydrogen evolution overpotential on the cobalt-rich alloys resulting in hydrogen evolution reactions taking place.

Partial polarization curves of Ni^{2+} and Co^{2+} co-deposition presented by Golodnitsky et al. indicated that at high Co concentrations, the curve is accompanied by the positive (0.2 V) shift of the cobalt reduction potential whilst the opposite effect (−0.5 V) was established for Ni (II) co-deposition [24]. This shift indicates that Co deposition is more favored at high concentrations of Co. At lower potentials, the Ni is favored, whilst at higher potentials, the reaction kinetics, enhanced by higher potential, favour Co over Ni. Fig. 5 depicts the SEM imaging of the cathode surface at different applied potential levels.

The cathode plate was found to have a non-sticking, spongy deposit at potentials higher than -1.25 Volts (Fig. 5(c–f)). Cleaning the cathodes was challenging since the porous layer of Co could be lost during cleaning, increasing the likelihood of an efficiency mistake. Electrowon deposit obtained when the applied potential was below or at the limiting

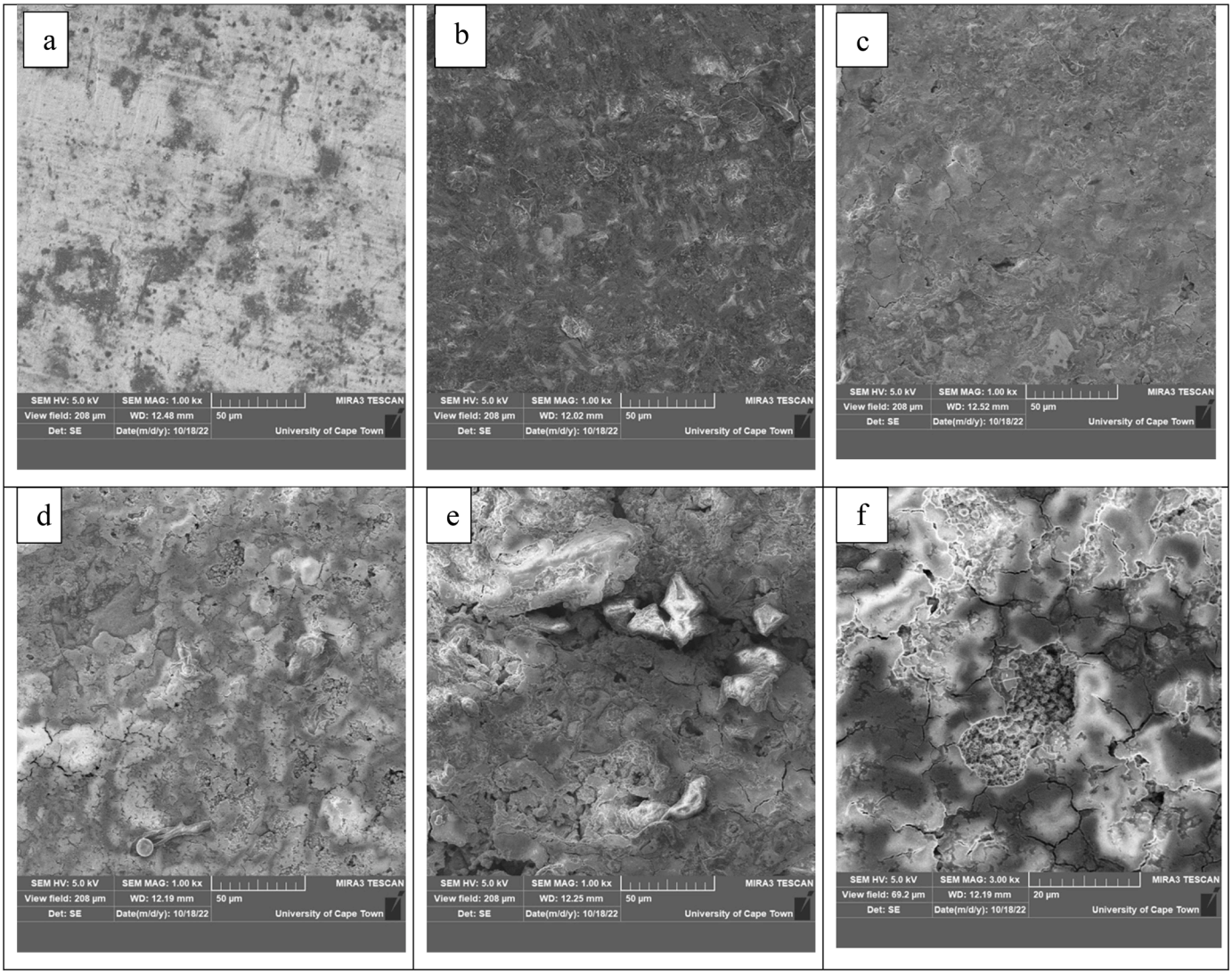

Fig. 5. SEM images of cathode surface after applying different potentials (a) 0 V (Fresh electrode), (b) -1.15 V, (c) -1.25 V, (d) -1.35 V, (e) and (f) -1.45 V vs Ag/AgCl (Deposit obtained in 30 g/L of $Co^{2+}_{0.3}Ni^{2+}_{0.7}$ solutions at pH=5, 70°C and 2 cm^2/250 cm^3 AA/EV).

potential (-1.15 V vs Ag/AgCl) resulted in a smooth, greyish and adherent deposit Fig. 5b). However, applying potential above the limiting potential produced an uneven, non-adherent, and nodular electrowon deposit, which denoted an unstable electrowinning system. The irregular-spongy deposit could be lost during washing, which would raise errors in the deposition rate and, as a result, reduce the apparent efficiency as it is now. In light of this, the limiting potential was established as -1.15 V vs Ag/AgCl for the next section of studies.

Effect of pH on current efficiency

Fig. 6 depicts the influence of the pH of the electrolyte on the Co-Ni electrodeposition current efficiency at different temperatures. The current efficiency rises sharply as the pH rises to around pH=3 (81 %), stabilizing between 3 and 5 and then decreasing sharply beyond 5. The current efficiency rises sharply as the pH rises to around pH=3 (81 %); then it stabilizes between 3 and 5 and then decreases sharply beyond 5. A similar trend was observed for the current efficiency and temp correlation at pH=4. It is also noteworthy that the average current efficiency is slightly higher at 50 °C than 60 °C due to the increased rate of the hydrogen evolution reaction, potentially lowering the selectivity for cobalt deposition.

At lower pH, the higher H^+ ion concentration results in substantial H_2 gas evolution at the cathode resulting in porous and poor morphology electrowon deposits that are poorly adherent to the Al cathode substrate. This subsequently results in poor current efficiency of the electrowon deposit. When pH is adjusted to levels higher than 5, the continuous consumption of H^+ ions (through H_2 gas evolution) and increased OH^- ions (from NaOH) at the cathode results in increased pH in the catholyte initiates $Co(OH)_2$ and $Ni(OH)_2$ precipitation [30]. The No and Co hydroxide precipitate gets incorporated in the electrowon deposit, resulting in a very poorly adherent and poor morphology deposit. Notably, the current efficiency steeply drops below pH 2.5 and more than 4.5. Hence a pH range of 3–4.5 appears to be reasonably optimal and satisfactory for good quality and adherent deposit, as further supported by enhanced current efficiency within the range.

Effect of temperature on current density and efficiency

Fig. 7 depicts the effect of temperature on the current efficiency at an applied potential of -1.15 V vs Ag/AgCl, pH=3, pH=4, pH=5 and pH=6 using an electrolyte composition of 30 g/L [$Co_{0.3}Ni_{0.7}$]. Generally, an increase in temperature leads to an increase in current efficiency across all pH levels up to 60 °C, indicating a positive temperature dependence. However, at higher temperatures (70 and 80 °C), the current efficiency begins to exhibit a decline, suggesting a potential temperature threshold beyond which the current efficiency diminishes, possibly due to unfavourable side reactions. Furthermore, the efficiency of the current is influenced by pH levels, and variations in the degree of improvement are evident across different pH values. The peak efficiency for each pH level occurs at different temperatures, emphasizing the interdependence between temperature, pH, and current efficiency in the electrochemical system studied.

The electrowinning data for cobalt deposition reveals compelling trends. The positive correlation between increasing temperature and current efficiency up to 60 °C is consistent with expectations in electrowinning, indicating enhanced kinetics at higher temperatures. However, the subsequent decline at 70 and 80 °C suggests a critical temperature threshold beyond which the benefits diminish, due to unfavourable side reactions (hydrogen evolution reaction and metallic hydroxide formation reaction). The mean current efficiency is significantly higher at pH=5 than pH =3 due to the decreased rate of the hydrogen evolution reaction, potentially improving the selectivity for cobalt deposition. The mean current efficiency is significantly lower at pH=3 than pH =6 due to the increased rate of the hydrogen evolution reaction and cobalt and nickel hydroxide formation reaction at pH=3 and pH=6 respectively, potentially lowering the selectivity for Co and Ni deposition. As depicted by Fig. 7(b), the highest current efficiency levels were recorded at temperatures between 50 °C and 60 °C and pH=4 and pH=5. The optimal values were chosen as 50 °C (to reduce energy consumption) and pH=4.5 (to reduce chemical consumption).

Electrowinning of Co-Ni alloys at higher temperatures enhanced both deposit quality and adherence, although the deposit generated at temperatures up to 40 °C was non-uniform and non-adherent. The

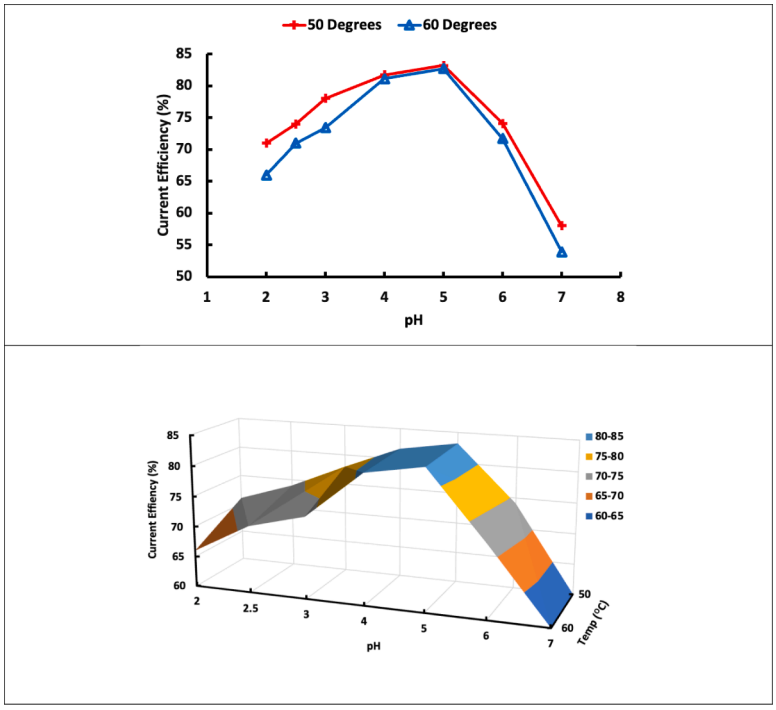

Fig. 6. Influence of pH of the electrolyte on Co-Ni electro-deposition at different temperatures (30 g/L $Co^{2+}_{0.3}Ni^{2+}_{0.7}$, 50 °C and 60 °C, -1.15 V vs Ag/AgCl and AA/EV of 2 cm^2/250 cm^3).

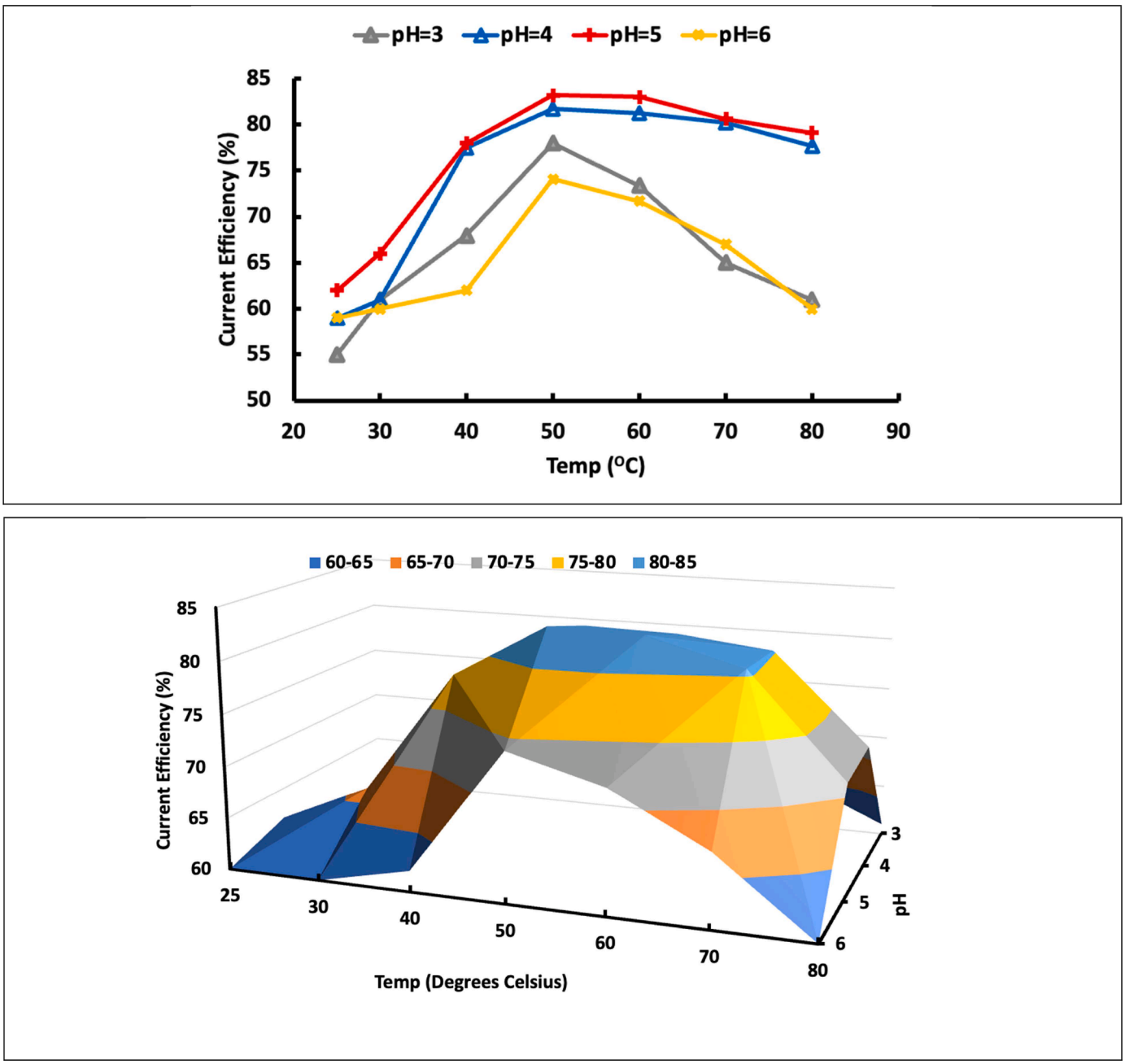

Fig. 7. The effect of temperature on the current efficiency at an applied potential of -1.15 V, at pH=3, pH=4, pH=5 and pH=6 using an electrolyte composition of 30 g/L [$Co^{2+}_{0.3}Ni^{2+}_{0.7}$] and AA/EV of 2 cm^2/250 cm^3.

enhanced ionic mobility at higher temperatures is what effectuates an increased current efficiency. The rapid fall of current efficiency from 70 °C is attributed to the decrease in hydrogen evolution overpotential on the cobalt-rich alloys resulting in a hydrogen evolution side reaction. This trend is also iterated with correlations by Lu et al. in which they demonstrated that the voltage needed to achieve the specified current density falls as the temperature rises [31]. The rapid availability of Co ions at the cathode can also result in less stressed, better-quality deposits [31,32]. Other factors, such as phase composition, affect the quality of the deposit. For example, Co can be found in both *a* and *h* forms, but the *h* form is favored since it is face-centered, and *a* form is hexagonally close-packed and not typically deposited in an electrowinning cell [33, 34].

It is asserted that the deposit will be *h* if made at higher temperatures and a mixture of *a* and *h* if made at lower temperatures which will undoubtedly put stress on the deposit and lead to its dissociation from the electrode [35]. Another issue with Co deposits is that in addition to Co (II), which is produced at the anode, Co (III) is also present in the electrolyte. Co_2O_3 powder was collected at the anode and examined using ferrous sulphate solutions in an oxidation–reduction process by Lakshminarayanan et al. [36] confirmed this. The presence of multivalent cations in the electrolyte causes a decrease in the efficiency and dendritic character of the deposit, even if the effects of Co (III) in the electrolyte are unknown. In order to generate Co-Ni deposits with acceptable morphology, a higher temperature of 50 °C was chosen.

Effect of concentration on Co-Ni concentration on current efficiency

Electrolysis was conducted by varying the cobalt-nickel concentration from 0 to 30 g/L in the presence of 10 g/L of monosodium phosphate at a temperature of 50 °C, pH=4 and applied potential of -1.15 V

(vs Ag/AgCl). The results, summarized in Fig. 8, shows that the current efficiency increases with increased cobalt concentration in the electrolyte.

It was also observed that electrowinning at low Co^{2+}-Ni^{2+} concentrations produces Co-Ni deposits that are stressed and brittle and ultimately stick loosely, quickly falling off from the Al cathode during electrowinning. This trend results in reduced current efficiency. Electrowinning at higher Co^{2+}-Ni^{2+} concentrations produces smoother, less brittle Co-Ni deposits that don't fall off easily from the Al cathode during electrowinning. This correlation arises due to the more abundant availability of Co^{2+}ions, vis-a`-vis hydrogen ions (H^{+}), at the higher Co^{2+}concentrations, while at lower Co concentrations, relatively higher H_2 evolution, and its consequent incorporation into the electrowon Ni-Co deposit, results not only in lower current efficiencies but also in brittle and stressed deposits. Since no additional benefit is derived in going beyond 25 g/L, a higher 30 g/L Co-Ni concentration value was chosen as the optimum Co-Ni concentration. The energy required to deposit cobalt also drops as the Co concentration increases. This is an obvious consequence of the lower voltage requirement (due to higher conductivity at the higher Ni-Co concentration levels) and the increased current efficiency.

Effect of monosodium phosphate on pH fluctuation

The tests were performed in a jacketed single-compartment reactor; however, there was significant pH variation during the experiments. A buffer was incorporated into the electrolyte solution to obtain higher current efficiency and an optimal way to limit the pH variation. Fig. 9 demonstrates the pH variation of the catholyte-anolyte solution during the experiment.

It can be observed that, except for the correlation related to a system

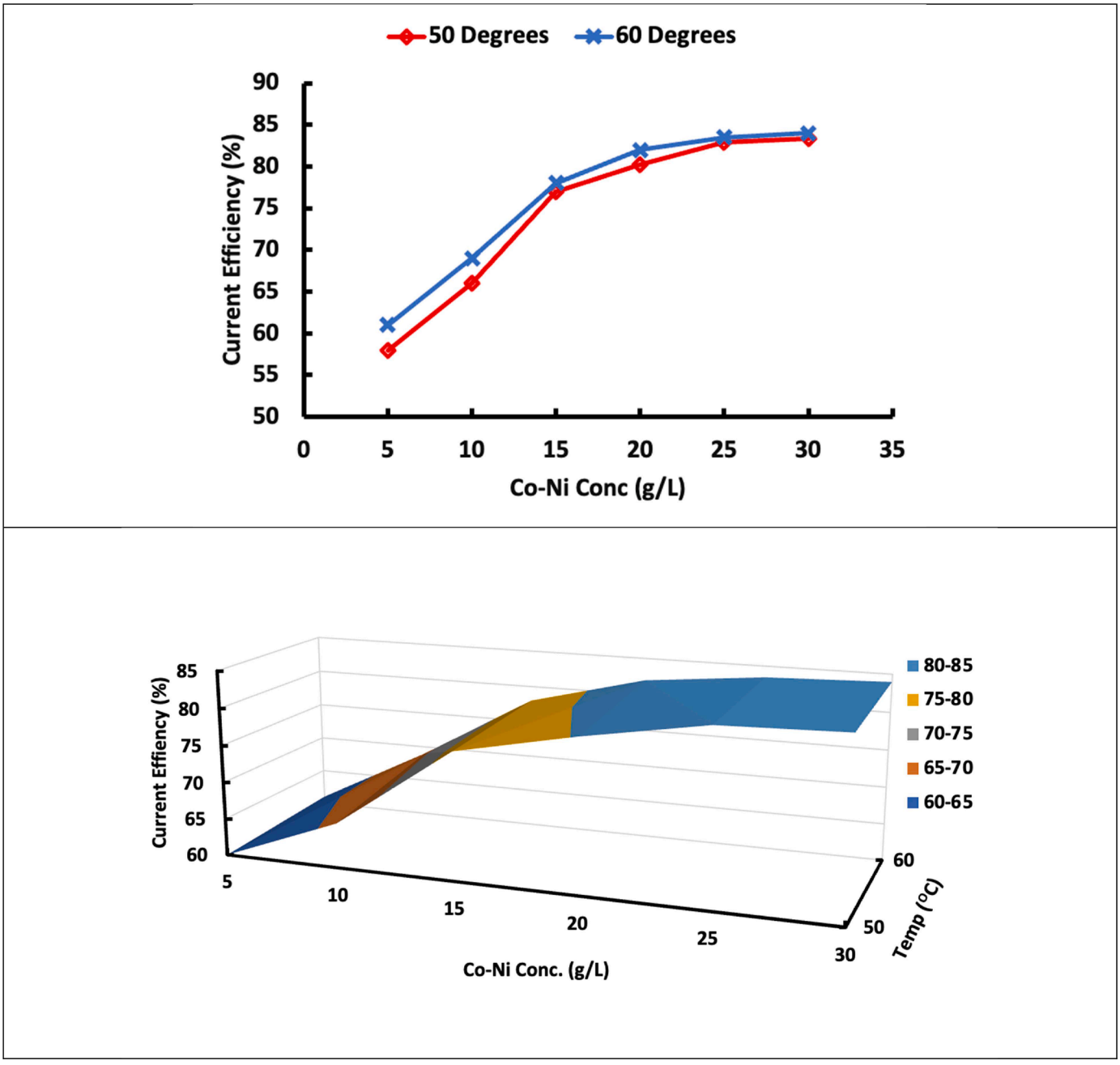

Fig. 8. Effect of Co concentration on the current efficiency at -1.15 V vs Ag/AgCl, pH=4.5, at 50 °C and 60 °C using a varied electrolyte composition up to 30 g/L [$Co^{2+}_{0.3}Ni^{2+}_{0.7}$] and AA/EV of 2 cm^2/250 cm^3.

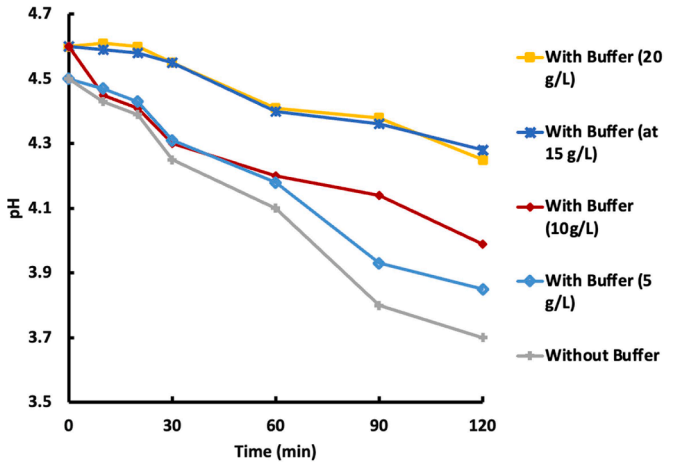

Fig. 9. pH variation with time in the electrowinning set-up at -1.15 V vs Ag/AgCl, 30 g/L [$Co^{2+}_{0.3}Ni^{2+}_{0.7}$], Starting pH=4.5, 50 °C and AA/EV of 2 cm^2/250 cm^3.

with buffer, the pH tends to decline during the investigation period. Excluding the effect of electrochemical reaction mechanisms and kinetics, these correlations also indicate that a higher solution temperature effectuates an increase in the proton migration and consumption rate as the pH decrease is much lesser in a higher temperature solution than in a lower temperature solution. The pH decreases rapidly from 4.5 to 3.7 after 120 min without using a monosodium phosphate buffer solution and less rapidly from 4.6 to 3.95 when monosodium phosphate is incorporated into the electrolyte solution.

This pH variation is possibly due to the water decomposition reaction on the anode electrode surface that yields oxygen gas and H^+ ions, which tend to migrate to the cathodic plate, where they accept electrons to produce H_2 gas. The continuous generation of H^+ at the anode decreases pH as the H^+ concentration in the electrolyte continues to increase. Thus, the pH variation for the test done at 50 °C could be explained as a function of the reaction rate difference between the rate of H^+ ions generation (from water oxidation) at the anode and the rate of H^+ rate of consumption (H_2 evolution) at the cathode. It is important to note at lower temperatures, the rate of the proton migration from the anolyte phase to the catholyte phase is reduced [37]. However, at higher temperatures, the H^+ migration is significantly increased due to increased kinetic mobility of protons, thereby intensifying the effect of the pH increase due to H_2 evolution, making the pH decrease less rapidly during the course of the tests since this effect counteracts the effect of pH decrease due to H^+ generation [37].

Fig. 9 illustrates the variation of the pH values during the electrowinning tests when varied doses (0–20 g/L) of monosodium phosphate are added to the electrolyte solution. The pH degradation decreases as the doses of monosodium phosphate increase. The pH decreased slightly from 4.5 to 4.2 after 120 min when monosodium phosphate buffer solution was utilized at 15 g/L. In the respective correlation, when electrowinning at 50 °C, it was observed that the pH falls at a rate much more accentuated than when monosodium phosphate is utilized. This effect confirms the buffer utilization efficiency in the pH control and, therefore, it also contributes to cost reduction, since it reduces the amount of chemical reactants necessary for the continuous pH adjustment. Evidently, monosodium phosphate addition effectuated improvements regarding the pH variation for the results obtained at 50 °C acting as a buffer. Regarding electrowinning at low temperatures, a negligible change could be observed in the pH variation when monosodium phosphate was added since little Co/Ni is expected to be deposited [37].

Effect of Na_2SO_4 on the current efficiency

The incorporation of an alkaline metal sulphate additive into the electrolyte solution increases the conductivity of the electrolyte solution medium. Experiments were performed by the addition of alkaline sulphates of sodium. The addition of a small amount of sodium sulphate resulted in an adherent and smooth Co-Ni composite deposit. The effect of sodium sulphate concentration on the current efficiency and solution overvoltage is depicted in Fig. 10.

As can be observed, the current efficiency increases and the solution overvoltage decreases with Na_2SO_4 addition up to 15 g/L, beyond which further addition of the salt exhibits little to negligible effect. The trend is largely due to solution electroconductivity induced by the free sulphate and sodium ions which act as charge carriers, therefore the more the amount of free and mobile ions, the higher the conductivity. The correlation is explicitly depicted by trends presented by Schalenbach et al. [38], which depicts the parametrization of the molar conductivity of Na_2SO_4 as a function of concentration. The increased molar conductivity results in lower H_2 evolution and higher efficiency for Co recovery. When the Na_2SO_4 concentration is increased above 15 g/L, there is a negligible drop in potential and a negligible increase in current efficiency. Lowering the applied potential and the increased current efficiency also results in lower energy requirements.

Effect of rotating cathode speed on current efficiency and current

The effects of cathode electrode rotation on the EW electrowinning performance were investigated by varying the cathode rotating speed from 0 to 40 rpm. As shown in Fig. 11a), the operating current density of the EW process increased from 0.018 ± 0.001 A/cm^2 (0 rpm) to 0.024± 0.001 A/cm^2 (20 rpm) and eventually to 0.35 ± 0.001 A/cm^2 (40 rpm).

This correlation in Fig. 11a) indicates a significant 74 % surge in the current density from 0 to 40 rpm. The deposition rate at 40 rpm was denoted to be 0.062 g/cm^2.h), which increased by 76% from the deposition rate at 0 rpm (0.035 g/cm^2.h). In addition, the cathode rotation speed played a significant role in effectuating turbulence in the electrolyte flow. This is reflected in the estimated Reynolds number (*Re*) that increased from 465 (10 rpm) to 1850 (40 rpm) using the equation:

$$N_{Re} = \frac{nD^2\rho_{sg}}{\mu_k} \tag{7}$$

Where n is impeller rotational speed (rev/s), D is impeller effective diameter (0.08 m), ρ_{sg} is the specific gravity (1.3) and μ_K is the kinematic viscosity (0.000003 m^2/s).

The turbulence in the electrolyte flow, indicated by a higher Reynolds number, can effectuate higher ionic and electronic mobility resulting in accelerated reduction reaction kinetics and less species

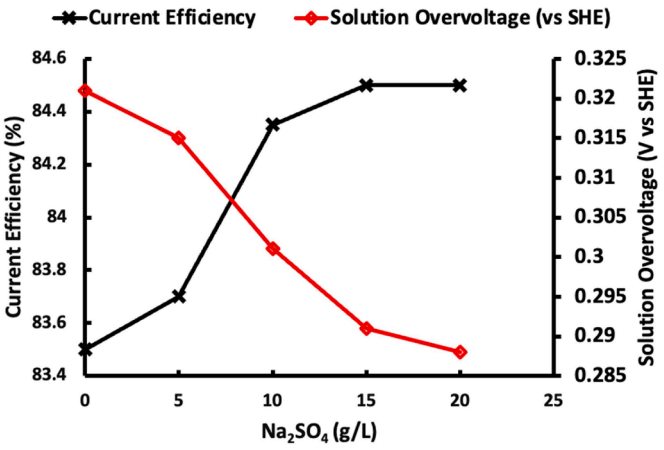

Fig. 10. Effect of Na_2SO_4 in an electrowinning set-up (-1.15 V, pH =4.5, 50 °C, 30 g/L $Co^{2+}_{0.3}Ni^{2+}_{0.7}$, 15 g/L NaH_2PO_4, AA/EV of 2 cm^2/250 cm^3).

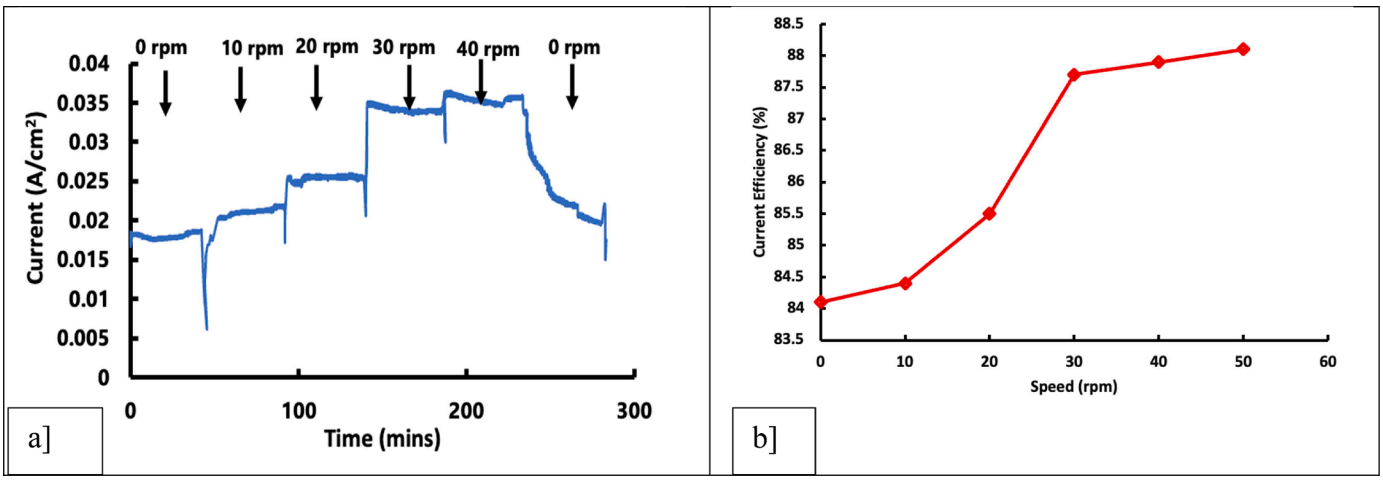

Fig. 11. (a) current as a function of rotating cathode speed and (b) the effect of cathode rotational speed on current efficiency (-1.15 V, pH =4.5, 50 °C, 30 g/L $Co^{2+}_{0.3}Ni^{2+}_{0.7}$, 15 g/L NaH_2PO_4, 15 g/L Na_2SO_4, AA/EV of 2 cm^2/250 cm^3).

build-up on the electrode-electrolyte interface per each level of potential. Meanwhile, the constant turbulent fluid motion also accelerates the diffusion and transfer of protons and anions from the anode surface film, thereby minimizing a localized pH gradient within the electrolyte-anode interphase. In addition, increased turbulence within the electrolyte flow can decrease the anodic and transport resistance for ionic species through to the cathode side, resulting in a higher current density [39, 40]. When the cathode rotation speed was set to 0 rpm, current density quickly decreased to 0.055 ± 0.02 A /cm^2, demonstrating that the cathode rotation speed played a significant role in the elevation of current density. The rotation speed of the also affected the current efficiency of Ni-Co deposition, as depicted in Fig. 11b).

Although the effect of rotating cathode speed on current efficiency was not immediately apparent between 0 rpm (84 %) and 10 rpm (84.5 %) since the current efficiency negligibly increased, further increasing the rotating speed gradually increased current efficiency to 85.5 % (20 rpm), 87.5 % (30 rpm), and 88 % (40 rpm). The correlational trend distinctly indicates that increasing cathode rotating speed results in a significant surge in the current efficiency. It is worth noting that the current efficiency increased significantly from 84 (0) to 88 (40 rpm).

Cobalt/Nickel electrowinning using synthetic sulphate solutions

Following completion of the electrowinning optimization experiments with synthetic solutions, which aimed to determine the ideal and optimal electrowinning conditions (-1.15 V vs Ag/AgCl, 47.5 g/L $Co^{2+}_{0.25}Ni^{2+}_{0.1}Mn^{2+}_{0.15}Li^{+}_{0.5}$, 50 °C, 15 g/L of NaH_2PO_4, 15 g/L Na_2SO_4, pH 4.5, 40 rpm), final electrowinning of Co-Ni was performed using the previously optimized conditions and parameters. The aluminium plate electrode was utilized as the cathode, and Pt coated Ti electrode as the anode. The physically stripped electrowon Co-Ni deposit exhibited smooth morphology and evenly distributed particle size and shape, as shown in Fig. 12e), and a significant part (>98 %) of it adhered to the cathode surface; therefore, it was feasible to easily calculate and quantify accurate current efficiency values.

In order to assess the best separation technique between constant current electrowinning and constant potential electrowinning, the deposit quality and composition were assessed. Optimal parameters for constant current electrowinning (CE) were noted from the approximated current response at the experimentally determined potential level whilst optimal potentiostatic electrowinning (PE) optimal parameters were experimentally determined in this work. As illustrated by Fig. 12a) constant current electrowinning at optimal current (0.035 A/cm^2) produced a deposit with lower purity (82% Ni-Co) than at constant potential, which produced 98% (Ni-Co). Constant potential electrowinning is more selective to specific reactions (Co and Ni reduction at -1.15 V vs Ag/AgCl) at a specific potential compared to constant current, which reduces relatively most of the cations in the solution. The lower purity of constant current electrowinning is primarily due to the deposited Mn, Li and Al and other impurities as confirmed by ICP and EDS analysis.

A graphical representation of how current efficiency varies over time is depicted in Fig. 12(b). The figure indicates that current efficiency decreases over time, this is attributed to the build-up of the non-conductive cobalt layer on the aluminium cathode plate and the decrease in the pH which promotes the hydrogen evolution side reaction.

In addition, Fig. 12(c) indicated that electrowinning of Ni-Co in a 30 g/L $Co_{0.3}Ni_{0.7}$ solution can be depleted to approximately 4.85 g/L g/L $Co_{0.33}Ni_{0.67}$ solution over a period of 180 min using two layered (3 × 10 cm^2) Pt coated Ti anodes and a rotating (3 × 10 cm^2) Aluminium plate electrode ((AA/EV ratio of 30 cm^2/250 cm^3). Since the electrodeposition reaction rate is solely dependent on one composite reactant (Co: Ni), as evident from Fig. 12c) and plot of ln*[A]* vs time in Fig. 12d) exhibit high degree of linearity, the electrowinning Co-Ni is deemed to be first order. The electrowinning first-order reaction proceeds according to the following reaction:

$$\ln[C_t] - \ln[C_0] = -kt \tag{8}$$

Where C_t is the concentration at any time, t, C_0 is the initial concentration, k is the reaction constant, and t is time. The reaction constant, k, is calculated to be 0.016 1/min, as depicted in Fig. 12d), bringing the first-order equation to the expression:

$$\ln[C_t] - \ln[C_0] = -0.016t$$

As per the kinetics correlation in Fig. 12d), the reaction kinetics correlation indicates a negative linear correlation between time and concentration. After 120 min, the electrodeposition stalls, as shown in Fig. 12c). This inactivity is attributed to less mass transfer gradient between the electrolyte and cathode surface due to depleted metallic ion species in the electrolyte, resulting in less metallic ion transfer from the electrolyte to the cathode electrode. In light of this, there is a need for continuous electrolyte replenishment; therefore, after 180 min of electrowinning, fresh new electrolyte is added to the electrowinning chamber.

Table 2 presents the elemental composition of the electrowon deposit as obtained by ICP-OES; it is evident that the composition of the electrowon deposit essentially constitutes Ni and Co (97 wt%). The preferential deposition of Co is prominent when AA/EV of 2 cm^2/250 cm^3 is utilized, however, when AA/AE of 30 cm^2/250 cm^3 is utilized, the

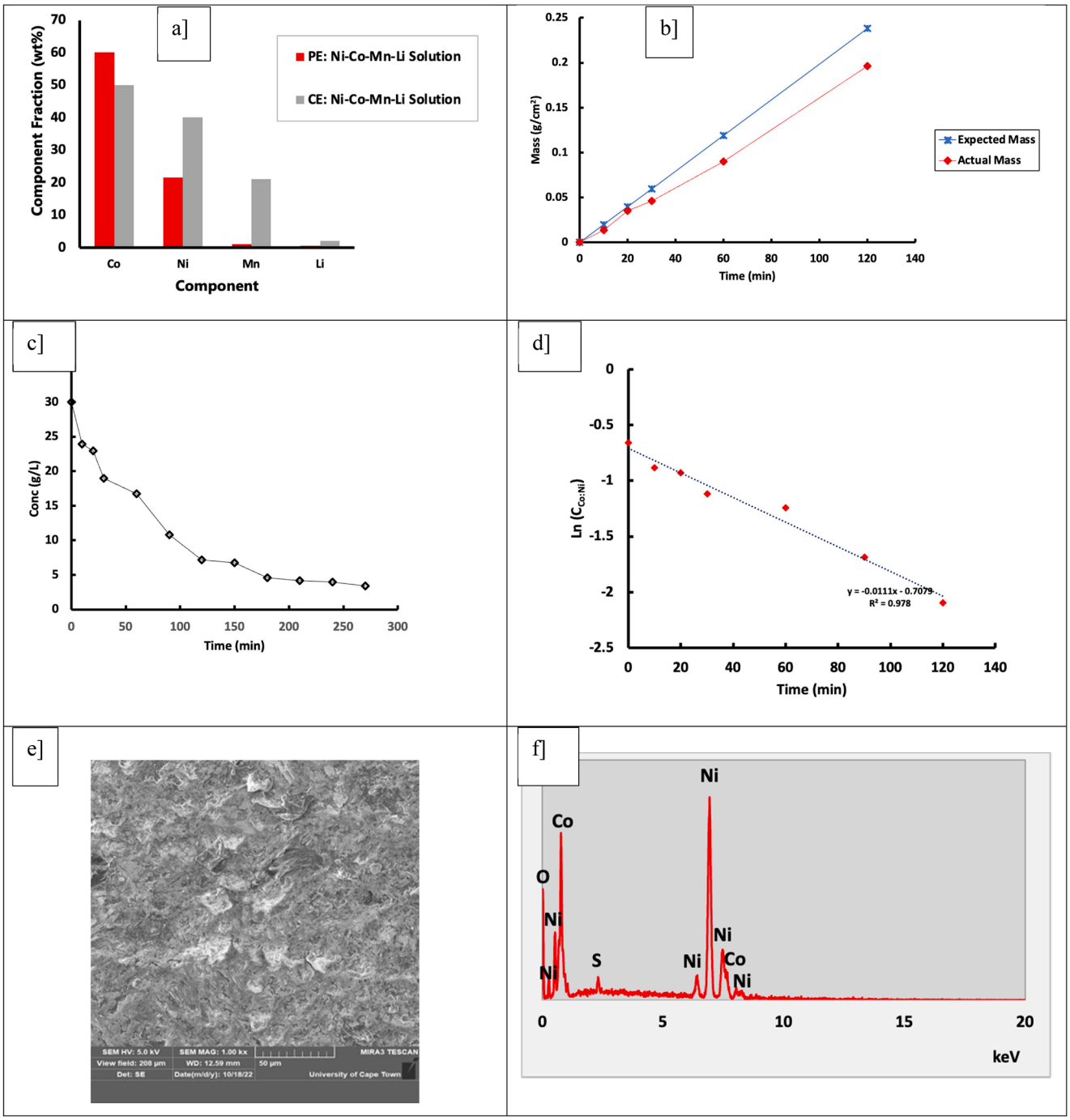

Fig. 12. (a) Composition of deposit from constant current electrowinning vs constant potential electrowinning (PE=>-1.15 V vs Ag/AgCl, 15 g/L NaH_2PO_4, 15 g/L Na_2SO_4, CE=> 0.035 A/cm^2, 2 cm^2/250 cm^3, 40 rpm, AA/EV in 47.5 $Co^{2+}_{0.25}Ni^{2+}_{0.1}Mn^{2+}_{0.15}Li^{+}_{0.5}$ Solution), (b) expected mass deposited vs actual mass deposited over 1 hour period (-1.15 V, pH =4, 50 °C, 30 g/L $Co^{2+}_{0.3}Ni^{2+}_{0.7}$, 15 g/L NaH_2PO_4, 15 g/L Na_2SO_4, 40 rpm, AA/EV of 2cm^2/250 cm^3), c) cconcentration variation of the 30 g/L $Co^{2+}_{0.3}Ni^{2+}_{0.7}$ synthetic solution over 250 min of electrowinning, d) Co-Ni electrodeposition reaction kinetics in the first 120 min (-1.15 V, pH =4.5, 50 °C, 30 g/L $Co^{2+}_{0.3}Ni^{2+}_{0.7}$, 40 rpm, 15 g/L NaH_2PO_4, 15 g/L Na_2SO_4, AA/EV of 30 cm^2/250 cm^3), (e) Micrograph of the deposit morphology, deposit obtained from the synthetic solution electrowinning and f) EDX spectrum of the deposit (-1.15 V vs Ag/AgCl, 50 °C, 40 rpm, 15 g/L of buffer, 15 g/L Na_2SO_4, pH 4.5,40 rpm, AA/EV of 30 cm^2/250 cm^3).

deposit composition consists of more Ni than Co. This correlation is due to the fact that at low AA/EV only a small cathode active area is exposed to the bulk electrolyte which therefore gives room to preferential Co deposition however this phenomenon is trumped at high AA/EV since the Co (in relatively smaller quantities compared to Ni) gets depleted quickly due increased deposition rate since the active is increased therefore Ni species won't have competing Co species during deposition for longer periods. As expected, Na traces (from NaOH and Na_2SO_4), Mn (from electrolyte) and Al traces (from Al cathode and cathode material) were co-deposited with Ni and Co as such impurities caused impurities

and possibly the deposit's relatively rough morphology qualities.

To determine whether the electrowon deposit was solely constituting metals listed in Table 2, an analysis by microprobe (EDX), presented in Fig. 12f) was performed.

The EDS analysis results are summarized in Fig. 12f) and demonstrate that no other metal was detected. However, they indicate the presence of other elements, such as oxygen, sulphur, and sodium.

The presence of oxygen and sulphur is probably associated with the contamination by the electrolyte solution. The presence of sulphur in the deposit is also an indirect indicator of sulfamate anion involvement in the cathodic reaction [24] In spite of the deposit, as presented in Fig. 12f), being rinsed and dried before the analysis, the cleaning process was possibly not effective in promoting the total removal of the solution contaminants. When the concentrations of the nonmetals are excluded, the Ni-Co composition concentration reaches 98.1 wt%, which was also confirmed by ICP-OES (98.2 wt%), which is more reliable.

Electrowinning cell voltage optimization

The cost of electrolysis constitutes the largest fragment of the total operational cost involved in the Co and Ni production. Therefore, great efforts are continuously being made in research to obtain the Co and Ni at a lower cost [1]. The total voltage of the cell (E) is a summated combination of the potential of various components, which include reaction potential (ER), as well as contributions from the anode potential (E_a), the anode overpotential (η_a), cathode potential (E_c), the cathode overpotential (the ohmic resistance of the electrolyte solution (E_{OE}), and the contact resistance (E_{CS}). The overall voltage is quantified as per the reaction equation:

$$E_E = E_a + |\eta_a| - (E_c + |\eta_c|) + E_{OE} + E_{CS}$$

For the electrolysis of Co and Ni with a conventional couple consisting of Pb and stainless-steel electrodes, the total calculated E is 2.8, and in practice, it ranges in the interval of 2.75–4 V [31–33,41,42]. Five Electrodes were selected as potential anodes for the electrowinning process, namely, glass carbon (C), graphite (GC), platinum (Pt), lead (Pb) and Titanium (Ti). Anodic overvoltage for the conventional Pb anode is 0.65 V vs Ag/AgCl, for glass carbon (C) is 1.6 V vs Ag/AgCl, for graphite (GC) 1.4 V vs Ag/AgCl, platinum (Pt) 0.25 V vs Ag/AgCl, and for Titanium (Ti) is 0.8 V vs Ag/AgCl. Pt exhibits the lowest overvoltage compared to other electrodes. The Pb electrode showed the least steady overpotential over the course of electrowinning. Fig. 13a depicts the anodic overvoltage for the 5 electrodes. Fig. 13(b) depicts the anodic overvoltage of Ti and Pt-coated Ti.

The cost factor, service life factor and corrosion factor (mass lost during operation) for all 5 electrodes were also integrated for comprehensive analysis (Fig. 13c)) Titanium appears to exhibit optimal well-rounded performance compared to other anodes. The capital cost of titanium is way lower than platinum, yet its service life and corrosion factor (mass loss per cm^2 per hour) are comparable to that of platinum.

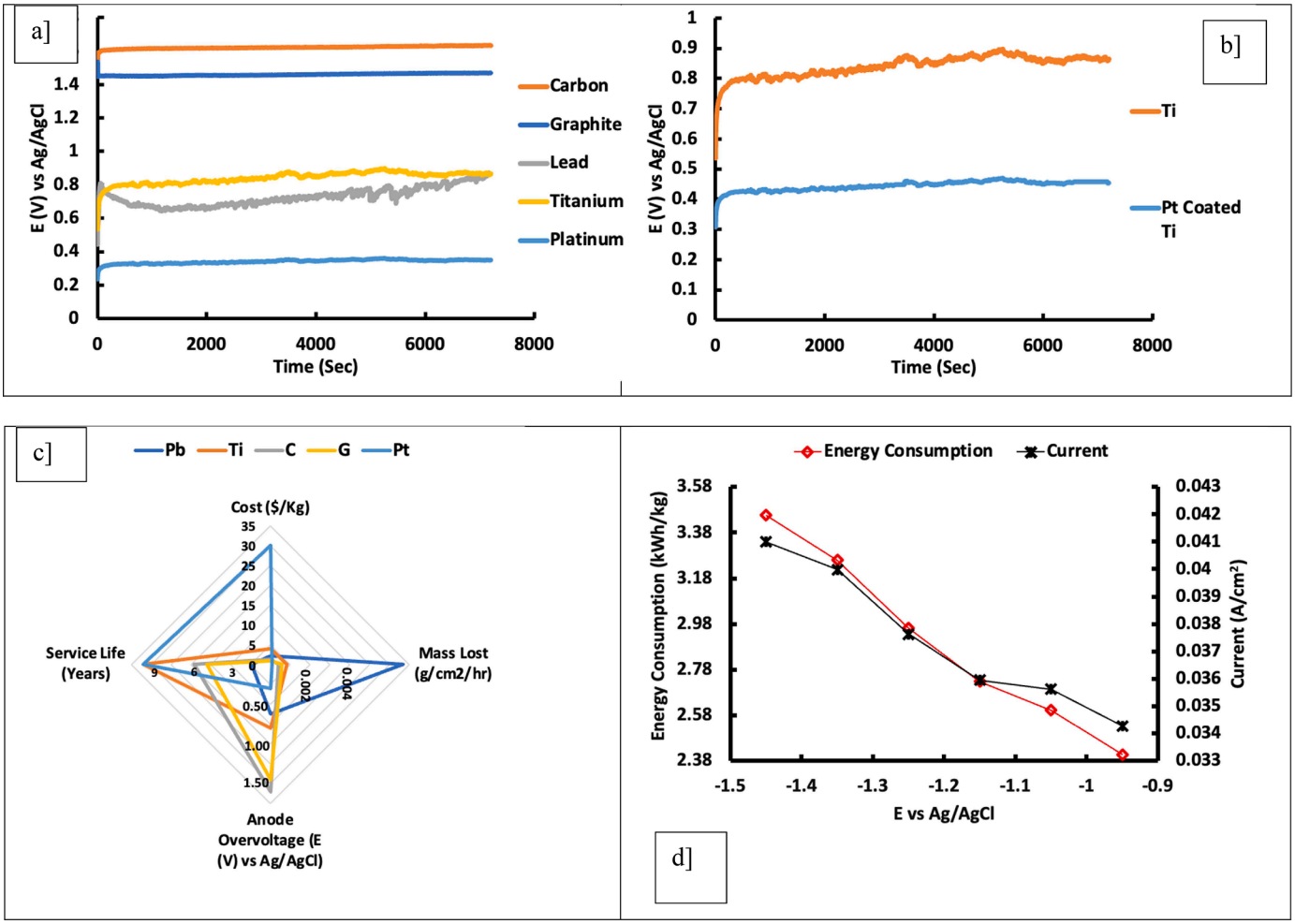

Fig. 13. (a) Anodic overvoltage for Pt, C, GC, Ti and Pb (0.035 A/cm^2, pH =4.5, 50 °C, 30 g/L $Co_{0.3}Ni_{0.7}$, 40 rpm, AA/EV of 2 cm^2/250 cm^3), (b) anodic overvoltage of Ti and Pt Coated Ti (0.035 A/cm^2, pH =4.5, 50 °C, 40 rpm, 15 g/L of buffer, 15 g/L Na_2SO_4, 40 rpm, 30 g/L $Co_{0.3}Ni_{0.7}$), c) Comprehensive performance analysis of pure Pb. Ti. Pt, C and GC electrodes based on anode overvoltage, cost, service life and corrosion factor (mass lost during operation) (Partial Data derived from ref (Bloomberg, 2022; Moradi et al., 2020) and (d) Specific energy consumption as a function of the current density for Co-Ni deposits.

Therefore, Pt plating of Ti which uses a relatively small amount of Pt can increase the service life whilst reducing the anodic overvoltage.

For platinum-coated titanium DSA, the anodic over-voltage decreased by 0.35 V when tested in 25 g/L $Co_{0.3}Ni_{0.7}$, at a pH of 4.5, and temperature of 50 °C as depicted in Fig. 13(b). Through the utilization of Pt-coated titanium, the conventional Pb anode will be replaced, but not the main oxidation reaction of water to produce oxygen, H^+ protons and free electrons. This transition leads to significant savings in specific energy consumption of the overall process and eliminates the classic conventional problem of acid mist formation in electrowinning cells. The results demonstrate that the proposed process generates 30 % less cell potential compared to conventional electrowinning cells. Per Ohms's law, a reduction of cell potential by 30% will also result in a reduction in the power consumption of the cell by 30% and, consequently the cost of operation. The anodic potential is determined to be 1.705 V vs SHE (1503 mV vs Ag/AgCl) at 0.035 A/cm^2, pH=4.5, 50 °C, 15 g/L of buffer, 15 g/L Na_2SO_4, 40 rpm and 30 g/L $Co_{0.3}Ni_{0.7}$.

$Ec + \eta c$ is the cathode potential. $Ec + \eta c$ recorded as -1.15 V (-0.895 V vs SHE) was obtained from data obtained from cyclic voltammetry and the effect of applied potential studies. The cathode overpotential of plating Co-Ni on Al was obtained by the potential difference between deposition potential (from CV) and the standard potential at cobalt deposition. The voltage drop caused by solution resistance can be calculated using current density and electrolyte conductivity. A suitable empirical equation for electrolyte conductivity was presented by Kargl-Simard et al.

$$\varepsilon = 103.86 - 0.29464[\mathrm{Co}] + 0.82661T + 0.91000\ [H_2SO_4] \quad (9)$$

Where ε is the electroconductivity (mS/cm), T is the temperature in degrees Celsius and $[H_2SO_4]$ is the H_2SO_4 concentration in g/L [43]. The conductivity of a 30 g/L ($Co_{0.3}Ni_{0.7}$) in 2 M H_2SO_4 (200 g/L), 50 °C electrolyte was calculated at 305 mS/cm (consistent with the measured value of 312 mS/cm). The current density of 350 A/m^2, electrode areas of 5cm^2 and a face-to-face anode to cathode separation of 0.025 m, the E_{OE} was calculated to be 0.287 V using the below equation.

$$E_{OE} = 1/\varepsilon \times L \times I \quad (10)$$

where ε is the specific conductivity of the electrolyte, L is the electrode gap, and I is the current density. The voltage component related to the contact resistance between electrode header bars and the cell busbars was also calculated to have a resistance of 58 $\mu\Omega$ for spool contacts [44]. Combining this with a 300 A/m^2 current density (5 cm^2 per electrode) at two contact points per cell (one anode and one cathode) produces a potential drop of 0.001 V.

$$E_{OE} = \Omega \times L \times I \quad (11)$$

where Ω is the specific conductivity of the electrolyte, L is the electrode effective length, and I is the current density.

Summating all the individual voltage components as shown in Table 3 produces a cell voltage of about 2.745 V which is significantly lower than commonly reported values which range between 3 and 4 V [41,42,45] The calculated energy consumption assumes no short circuits and does not include electrical consumption due to rectification and resistances in the electrical bus system.

Table 3
Cell voltage contributions from anode potential, cathode potential, solution voltage and contact voltage.

Component	Value (V vs SHE)	Percentage Contribution (%)
Anodic Potential ($E_a + \lvert\eta_a\rvert$)	1.605	57
Cathodic Potential ($E_c - \lvert\eta_c\rvert$)	-0.895	32
Solution Resistance Potential (E_{OE})	0.287	10
Contact Resistance Potential (E_{CS})	0.001	0.0004
Total Voltage	2.785	

In the scope of the parameters explored and optimised in this investigation, the lowest energy consumption (2.72 kWh/kg), as indicated in Fig. 13d), was derived utilizing the optimised cell voltage of 2.785 V and a current density of 0.035 A/cm^2 (350 A/m^2). The relatively minimized energy consumption does not consider corrosion, production rate and other operational limitations. On average, the total energy consumption during cobalt electrowinning is typically around 3 kWh/kg, varying within the range of 2.8 to 3.4 kWh/kg, while utilising a current density of 300 A/m^2. This work presents an approximately 14% decrease in energy consumption whilst operating at approximately 16% more current density and 88% current efficiency. Based on the production capacities of the primary cobalt electrowinning operations worldwide, which summed up to around 185,000–195,000 tons per year in 2019, the energy consumption for the electrowinning stage of electrolytically refined cobalt was estimated to be about 580–650 million kWh annually [46]. In light of this, reducing the total energy demand by 1 % would lead to energy savings of approximately 6 million kWh within a year.

Conclusions

The results demonstrate the feasibility of Ni-Co recovery from synthetic Li, Ni, Mn and Co sulphate solutions using selective potentiostatic electrowinning. The process model is aimed at being applied in closed and open loop spent Li-ionB cathode recycling process. In this work, Ni-Co alloys from synthetic NMC 532 leachate solutions were recovered through an integrated hydrometallurgy and electrometallurgy process for closed and open-loop recycling since besides cathode production, Ni-Co alloys and alloys can also be used in magnetic films, electrocatalysis, electronic chips, anti-corrosion systems, micro and nanogears among other various technological applications [15,16]. Ni-Co is recovered as composite material since separation of Co from Ni using conventional solvent extraction processes is both cost and energy-intensive and Co-Ni composite can be fed directly to both the conventional anhydrous and hydrous cathode production processes therefore this stage of processing can be eliminated. The leaching parameters S/L ratio, temperature, acid and oxidant concentration and leaching time were successfully optimized to recover > 98 % of the metal constituted in the cathode. The electrowinning parameters applied potential, temperature, pH, Co-Ni, Na_2SO_4 and buffer concentration, and electrode distance and active area were successfully optimized to recover 0.060 g/cm^2.h at 88 % current efficiency.

The leaching parameters S/L ratio, temperature, acid and oxidant concentration and leaching time were successfully optimized to recover > 97 % of the metal constituted in the cathode material (NMC 532). The composition of a typical NMC 532 cathode was noted and an identical synthetic solution was made to effectively study the selective electrowinning process. The electrowinning parameters-applied potential, temperature, pH, Co-Ni, Na_2SO_4 and NaH_2PO_4 buffer concentration and cathode rotational speed were successfully optimized to recover 97.2 % pure $Ni_{0.65}Co_{0.35}$ at 0.06 g/cm^2.h at 88 % current efficiency. The $Ni_{0.65}Co_{0.35}$ composite will be reacted with H_2SO_4 to produce $NiSO_4$–$CoSO_4$ salt for the hydrous NMC production plants. The anhydrous NMC production plants can utilize pure Ni-Co powder.

The optimum process conditions that yielded 88 % current efficiency and ideal deposit cohesion for Ni-Co deposition were: conditions (-1.15 V vs Ag/AgCl, 37.5 g/L Co-Ni-Mn, 50 °C, 15 g/L of monosodium phosphate buffer, 15 g/L Na_2SO_4, pH 4.5) following the leaching at 75 g/L S/L, 2 M H_2SO_4 + 6 H_2O_2 v/v% solution, at 60 °C for 2 h. 90% of the Co and 75% of the Ni in the leachate was recovered in a 3 hr electrowinning run. The Ni-Co composite will be reacted with H_2SO_4 acid in the ratio of 55 $g_{Ni\text{-}Co}$/L of 2 M H_2SO_4 solution at room temperature and pressure to yield its respective sulphate salts. The findings successfully

demonstrated the technical feasibility of Ni-Co composite recovery can be recovered from spent electrolytes through selective electrowinning.

Funding

Funding provided by the Department of Science and Innovation through Waste RDI Roadmap Grant CSIR/BEI/WRIU/2021/052 in order to execute this research project is gratefully acknowledged. Finally, financial and strategic support received through the South African National Energy Development Institute (SANEDI) and the Energy & Water Sector Education Training Authority (EWSETA) in South Africa is greatly appreciated.

CRediT authorship contribution statement

Tendai Tawonezvi: Writing – review & editing, Writing – original draft, Visualization, Validation, Supervision, Resources, Methodology, Formal analysis, Conceptualization. **Dorcas Zide:** Writing – review & editing, Supervision, Methodology, Conceptualization, Validation. **Myalelo Nomnqa:** Writing – review & editing, Supervision, Methodology, Conceptualization, Resources. **Leslie Petrik:** Writing – review & editing, Supervision, Methodology, Conceptualization, Funding acquisition. **Bernard Jan Bladergroen:** Writing – review & editing, Supervision, Methodology, Conceptualization, Funding acquisition.

Declaration of competing interest

The authors declare that they have no known competing financial interests or personal relationships that could have appeared to influence the work reported in this paper.

Data availability

Data will be made available on request.

Acknowledgments

Funding provided by the Department of Science and Innovation through Waste RDI Roadmap Grant CSIR/BEI/WRIU/2021/052 in order to execute this research project is gratefully acknowledged. Finally, financial and strategic support received through the South African National Energy Development Institute (SANEDI) and the Energy & Water Sector Education Training Authority (EWSETA) in South Africa is greatly appreciated.

References

[1] T. Tawonezvi, M. Nomnqa, L. Petrik, B.J. Bladergroen, Recovery and recycling of valuable metals from spent lithium-ion batteries: a comprehensive review and analysis, Energies 16 (3) (2023) 1365, https://doi.org/10.3390/en16031365 (Basel)Jan.
[2] X. Zeng, J. Li, N. Singh, Recycling of spent lithium-ion battery: a critical review, Crit. Rev. Environ. Sci. Technol. 44 (10) (2014) 1129–1165, https://doi.org/10.1080/10643389.2013.763578. May.
[3] N. Nitta, F. Wu, J.T. Lee, G. Yushin, Li-ion battery materials: present and future, Mater. Today 18 (5) (2015) 252–264, https://doi.org/10.1016/J.MATTOD.2014.10.040. Jun.
[4] J. Neumann, et al., Recycling of lithium-ion batteries—current state of the art, circular economy, and next generation recycling, Adv. Energy Mater. 12 (17) (2022), https://doi.org/10.1002/aenm.202102917. May.
[5] D. Werner, U.A. Peuker, T. Mütze, Recycling chain for spent lithium-ion batteries, Metals 10 (3) (2020) 316, https://doi.org/10.3390/met10030316 (Basel)Feb.
[6] Phuc Anh L.E., "The recyclability of lithium-ion battery materials," THE UNIVERSITY OF Q UEENSLAND, ST LUCIA, 2019. Accessed: Jan. 22, 2023. [Online]. Available: https://core.ac.uk/download/pdf/286812476.pdf.
[7] T. Kim, W. Song, D.Y. Son, L.K. Ono, Y. Qi, Lithium-ion batteries: outlook on present, future, and hybridized technologies, J. Mater. Chem. A 7 (7) (2019) 2942–2964, https://doi.org/10.1039/C8TA10513H. Royal Society of Chemistry.
[8] Kelleher Environmental, "Research study on reuse and recycling of batteries employed in electric vehicles: the technical, environmental, economic, energy and cost implications of reusing and recycling EV batteries," Ontario, Canada, 2019.
[9] ESMAP, "Reuse and recycling: environmental sustainability of lithium-ion battery energy storage systems an energy storage partnership report," 2022. [Online]. Available: www.worldbank.org.
[10] J. Piątek, S. Afyon, T.M. Budnyak, S. Budnyk, M.H. Sipponen, A. Slabon, Sustainable Li-ion batteries: chemistry and recycling, Adv. Energy Mater. 11 (43) (2021), 2003456, https://doi.org/10.1002/aenm.202003456. Nov.
[11] M.T. Islam, U. Iyer-Raniga, Lithium-ion battery recycling in the circular economy: a review, Recycling 7 (3) (2022) 33, https://doi.org/10.3390/recycling7030033. May.
[12] V. Chandran, et al., Comprehensive review on recycling of spent lithium-ion batteries, Mater. Today Proc. 47 (2021) 167–180, https://doi.org/10.1016/j.matpr.2021.03.744.
[13] T. Yang, D. Luo, A. Yu, Z. Chen, Enabling future closed-loop recycling of spent lithium-ion batteries: direct cathode regeneration, Adv. Mater. (2023), https://doi.org/10.1002/adma.202203218. Apr.
[14] M. Chen, et al., Closed loop recycling of electric vehicle batteries to enable ultra-high quality cathode powder, Sci. Rep. 9 (1) (2019) 1654, https://doi.org/10.1038/s41598-018-38238-3. Feb.
[15] L. Tian, J. Xu, C. Qiang, The electrodeposition behaviors and magnetic properties of Ni–Co films, Appl. Surf. Sci. 257 (10) (2011) 4689–4694, https://doi.org/10.1016/j.apsusc.2010.12.123. Mar.
[16] A. Karimzadeh, M. Aliofkhazraei, F.C. Walsh, A review of electrodeposited Ni-Co alloy and composite coatings: microstructure, properties and applications, Surf. Coat. Technol. 372 (2019) 463–498, https://doi.org/10.1016/j.surfcoat.2019.04.079. Aug.
[17] C.R.K. Rao, M. Pushpavanam, Electroless deposition of platinum on titanium substrates, Mater. Chem. Phys. 68 (1–3) (2001) 62–65, https://doi.org/10.1016/S0254-0584(00)00268-6. Feb.
[18] D. de Castro, I. dos Santos, M. Mansur, A. Dutra, Voltammetric study on the electrowinning of cobalt in the presence of additives, J. Braz. Chem. Soc. (2023), https://doi.org/10.21577/0103-5053.20230048.
[19] J.T. Matsushima, F. Trivinho-Strixino, E.C. Pereira, Investigation of cobalt deposition using the electrochemical quartz crystal microbalance, Electrochim. Acta 51 (10) (2006) 1960–1966, https://doi.org/10.1016/j.electacta.2005.07.003. Feb.
[20] G.A. Kozhina, A.N. Ermakov, V.B. Fetisov, A.V. Fetisov, K. Yu. Shunyaev, Electrochemical dissolution of Co_3O_4 in acidic solutions, Russ. J. Electrochem. 45 (10) (2009) 1170–1175, https://doi.org/10.1134/S1023193509100097. Oct.
[21] M. Nusheh, H. Yoozbashizadeh, Studyon electrowinningofcobaltbycyclic voltammetrytechnique, Iran. J. Mater. Sci. Eng. V 7 (2) (2009).
[22] T. Brousse, D. Bélanger, J.W. Long, To be or not to be pseudocapacitive? J. Electrochem. Soc. 162 (5) (2015) A5185–A5189, https://doi.org/10.1149/2.0201505jes. Mar.
[23] Ma. Reyes-Valderrama, et al., Urban mining and electrochemistry: cyclic voltammetry study of acidic solutions from electronic wastes (printed circuit boards) for recovery of Cu, Zn, and Ni, Metals 7 (2) (2017) 55, https://doi.org/10.3390/met7020055 (Basel)Feb.
[24] D. Golodnitsky, N.V. GudinG, G.A. Volyanuk, Cathode process in nickel-cobalt alloy deposition from sulfamate electrolytes - application to electroforming, Plating Surf. Finish. 85 (2) (1998).
[25] N. Zech, E.J. Podlaha, D. Landolt, Anomalous codeposition of iron group metals: I. Experimental results, J. Electrochem. Soc. 146 (8) (1999) 2886–2891, https://doi.org/10.1149/1.1392024. Aug.
[26] J.K. Burdett, G.D. Price, S.L. Price, Role of the crystal-field theory in determining the structures of spinels, J. Am. Chem. Soc. 104 (1) (1982) 92–95, https://doi.org/10.1021/ja00365a019. Jan.
[27] A. Doroshenko, "Synthesis of metallophosphonate molecular and polymeric complexes, the study of their properties and reactivity," 2019.
[28] S.J. Chadwell, D. Rickard, G.W. Luther, Electrochemical evidence for pentasulfide complexes with Mn2+, Fe2+, Co2+, Ni2+, Cu2+ and Zn2+, Aquat. Geochem. 5 (1) (1999) 29–57, https://doi.org/10.1023/A:1009611719625.
[29] S.J. Chadwell, D. Rickard, G.W. Luther, Electrochemical evidence for metal polysulfide complexes: tetrasulfide (S2-4) reactions with Mn2+, Fe2+, Co2+, Ni2+, Cu2+, and Zn2+, Electroanalysis 13 (1) (2001) 21–29, https://doi.org/10.1002/1521-4109(200101)13:1<21::AID−ELAN21>3.0.CO;2-P. Jan.
[30] M.I. Jeffrey, W.L. Choo, P.L. Breuer, The effect of additives and impurities on the cobalt electrowinning process, Miner. Eng. 13 (12) (2000) 1231–1241, https://doi.org/10.1016/S0892-6875(00)00107-2. Oct.
[31] J. Lu, D. Dreisinger, T. Glück, Cobalt electrowinning – a systematic investigation for high quality electrolytic cobalt production, Hydrometallurgy 178 (2018) 19–29, https://doi.org/10.1016/j.hydromet.2018.04.002. Jun.
[32] I.G. Sharma, P. Alex, A.C. Bidaye, A.K. Suri, Electrowinning of cobalt from sulphate solutions, Hydrometallurgy 80 (1–2) (2005) 132–138, https://doi.org/10.1016/j.hydromet.2005.08.003. Nov.
[33] N. Pradhan, P. Singh, B.C. Tripathy, S.C. Das, Electrowinning of cobalt from acidic sulphate solutions—effect of chloride ion, Miner. Eng. 14 (7) (2001) 775–783, https://doi.org/10.1016/S0892-6875(01)00072-3. Jul.
[34] T. Cohen-Hyams, W.D. Kaplan, J. Yahalom, Structure of electrodeposited cobalt, Electrochem. Solid State Lett. 5 (8) (2002) C75, https://doi.org/10.1149/1.1491335.
[35] T. Mehmood, B.S. Khan, A. Mukhtar, M. Tan, Influence of bath temperature and pH on the structure of electrodeposited cobalt nanowires, Int. J. Mater. Res. 106 (9) (2015) 957–961, https://doi.org/10.3139/146.111269. Sep.

[36] G.R. Lakshminarayanan, E.S. Chen, J.C. Sadak, F.K. Sautter, Electrodeposition of cobalt using an insoluble anode, J. Electrochem. Soc. 123 (11) (1976) 1612–1616, https://doi.org/10.1149/1.2132656. Nov.
[37] J.S. Santos, R. Matos, F. Trivinho-Strixino, E.C. Pereira, Effect of temperature on Co electrodeposition in the presence of boric acid, Electrochim. Acta 53 (2) (2007) 644–649, https://doi.org/10.1016/j.electacta.2007.07.025. Dec.
[38] M. Schalenbach, Y.E. Durmus, H. Tempel, H. Kungl, R.A. Eichel, Ion transport and limited currents in supporting electrolytes and ionic liquids, Sci. Rep. 12 (1) (2022) 6215, https://doi.org/10.1038/s41598-022-10183-2. Apr.
[39] T.H.J.A. Sleutels, R. Lodder, H.V.M. Hamelers, C.J.N. Buisman, Improved performance of porous bio-anodes in microbial electrolysis cells by enhancing mass and charge transport, Int. J. Hydrog. Energy 34 (24) (2009) 9655–9661, https://doi.org/10.1016/j.ijhydene.2009.09.089. Dec.
[40] Y. Pan, T. Zhu, Z. He, Energy advantage of anode electrode rotation over anolyte recirculation for operating a tubular microbial fuel cell, Electrochem. Commun. 106 (2019), 106529, https://doi.org/10.1016/j.elecom.2019.106529. Sep.
[41] A. Kazem-Ghamsari, H. Abdollahi, Electrowinning of nickel and cobalt from non-circulated sulfate electrolyte, Trans. Indian Inst. Met. 75 (5) (2022) 1141–1151, https://doi.org/10.1007/s12666-021-02457-6. May.
[42] N. Mulaudzi, M.H. Kotze, Direct cobalt electrowinning as an alternative to intermediate cobalt mixed hydroxide product, in: Proceedings of the Southern African Institute of Mining and Metallurgy Base Metals Conference, Mpumalanga: The Southern African Institute of Mining and Metallurgy, 2013. Sep.
[43] C. Kargl-Simard, J.H. Huang, A.M. Alfantazi, Electrical conductivity and density of CoSO4/H2SO4 solutions in the range of modern cobalt electrowinning electrolytes, Miner. Eng. 16 (6) (2003) 529–535, https://doi.org/10.1016/S0892-6875(03)00059-1. Jun.
[44] T. Battle, M. Moats, A. Allanore, Ni-Co 2013, Springer International Publishing, Cham, 2016, https://doi.org/10.1007/978-3-319-48147-0.
[45] R. Carvajal Ortiz, T. Amietszajew, R. Bhagat, Recovery of nickel and cobalt by electrowinning from spent lithium-ion batteries using molten salt electrolytes, ECS Meet. Abstr. MA2020-02 (18) (2020), https://doi.org/10.1149/MA2020-02181536mtgabs, 1536–1536Nov.
[46] D. Talan, Q. Huang, A review study of rare Earth, Cobalt, Lithium, and Manganese in Coal-based sources and process development for their recovery, Miner. Eng. 189 (2022), 107897, https://doi.org/10.1016/j.mineng.2022.107897. Nov.